

ROTATIONALLY TIME-RESOLVED VIS-SPECTROSCOPY OF (3200) PHAETHON

Daisuke Kinoshita

Institute of Astronomy, National Central University, 300 Jhongda Rd., Chungli, Taoyuan,
320, Taiwan

Katsuhiro Ohtsuka

Tokyo Meteor Network, Daisawa 1-27-5, Setagaya, Tokyo, 155-0032, Japan

ohtsuka@jb3.so-net.ne.jp

Takashi Ito

Center for Computational Astrophysics, National Astronomical Observatory of Japan,
Osawa 2-21-1, Mitaka, Tokyo, 181-8588, Japan

Seidai Miyasaka

Tokyo Metropolitan Government, Nishi-Shinjuku 2-8-1, Shinjuku, Tokyo, 163-8001, Japan

Tomoki Nakamura

Department of Earth science, Graduate School of Science, Tohoku University, 6-3,
Aramaki Aza Aoba, Aoba, Sendai, Miyagi 980-8578, Japan

Shinsuke Abe

Department of Aerospace Engineering, Nihon University, 7-24-1, Narashinodai, Funabashi,
Chiba 274-8501, Japan

Wen-Ping Chen

¹Last updated: March 2, 2017

Institute of Astronomy, National Central University, 300 Jhongda Rd., Chungli, Taoyuan,
320, Taiwan

Received _____; accepted _____

ABSTRACT

Apollo-type near-Earth asteroid (3200) Phaethon, classified at the B/F-type taxonomy, probably the main mass of the Phaethon-Geminid stream complex (PGC), can be the most metamorphic C-complex asteroid in our solar system, since it is heated up to ~ 1000 K by the solar radiation heating around its perihelion passages. Hence, the surface material of the asteroid may be easily decomposed in near-sun environment. Phaethon's spectrum exhibits extremely blue-slope in the VIS-NIR region (so-called Phaethon Blue). Another candidate large member of the PGC, Apollo asteroid (155140) 2005 UD, shows a B/F-type color, however with a C-type-like red color over its $\sim 1/4$ rotational part, which implies an exposition of less metamorphosed primordial internal structure of the PGC precursor by a splitting or breakup event long ago. If so, some rotational part of Phaethon should show the C-type color as well as 2005 UD. Hence, we carried out the time-series VIS-spectroscopic observations of Phaethon in 30 November– 2 December, 2007, using 1-m telescope at Lulin observatory in Taiwan in order to detect such a signature on Phaethon. Also, *R*-band photometries were simultaneously performed in order to complement our spectroscopy. Consequently, we obtained a total of 68 VIS-spectrophotometric data, 78% of which show the B-type blue-color, as against the rest of 22% showing the C-type red-color, as we expected. We successfully acquired rotationally time-resolved spectroscopic data, of which particular rotational phase shows a red-spectral slope as the C-type color, as 2005 UD does, suggesting longitudinal inhomogeneity on Phaethon's surface. We constrained this C-type red-colored area in the mid-latitude in Phaethon's southern hemisphere based on the rotationally time-resolved spectroscopy along with Phaethon's axial rotation state, of which size suggests the impact-induced origin of the PGC. We also surveyed the meteoritic

analog of Phaethon’s surface blue-color, and found thermally metamorphosed CI/CM chondrites as likely candidates.

Subject headings: minor planets, asteroids: individual (3200 Phaethon, 155140 2005 UD) — meteorites, meteors, meteoroids — techniques: spectroscopic, photometric — methods: observational — Planetary systems

1. Introduction

Near-Earth asteroids (NEAs) come around the inner solar system from various source regions, bringing materials and information that serve as important clues to understand the origin and evolution of the solar system environment. Some of them may be extinct or dormant cometary nuclei, coming from the Jupiter family comet (JFC) region. Apollo-type NEA (3200) Phaethon (= 1983 TB: Green & Kowal 1983) has been well-known as one of the most enigmatic small bodies in the solar system, since it involves the Phaethon-Geminid stream complex (hereafter, PGC: Whipple 1983; Babadzhanov & Obrubov 1992; Kasuga 2009) even though Phaethon is not a comet but an asteroid. So, the asteroid has long been regarded as an extinct cometary nucleus. However, the recent dynamical study by de León et al. (2010) revealed that Phaethon was possibly chipped out from Main-belt asteroid (2) Pallas within ~ 30 Myr, i.e., within a typical dynamical lifetime of NEAs (Gladman et al. 1997; Ito & Malhotra 2010). This fact practically denies a cometary origin of Phaethon. The asteroid is not only an NEA but also a near-Sun asteroid (NSA). Its eccentricity e , semimajor axis a , and perihelion distance q are respectively $e = 0.89$, $a = 1.27$ AU, and $q = 0.14$ AU at the present evolutionary epoch, thus the relativistic effects of the Sun is not negligible when we study long-term dynamical evolution of Phaethon (Galushina et al. 2015): more effective than the Yarkovsky effect on the asteroid. Since Phaethon's orbital plane is moderately inclined to the ecliptic plane at inclination, $i \sim 22^\circ$, the q - i oscillating (and e at antiphase) secular evolution is controlled under the Lidov–Kozai circulation mechanism with the ω -cycle of $\sim 37,000$ yr (Urakawa et al. 2014).

Dynamical and physical behaviors of NSAs and small solar system bodies (hereafter, SSSB(s)) in near-sun environments have recently drawn our particular interest (Jewitt 2013). Phaethon is currently the largest object, $D \simeq 5.1$ km in size (Harris 1998; Hanuš et al. 2016a), among all the known NSAs. The asteroid should suffer strong solar

radiation heating around its perihelion passages, where sub-solar surface temperature of Phaethon is estimated to be at 800–1100 K (Ohtsuka et al. 2009) from FRM (Fast Rotating Model: Lebofsky & Spencer 1989) and NEATM (Near-Earth Asteroid Thermal Model: Harris 1998). This temperature is high enough to metamorphose primitive chondritic materials that have never undergone high-temperature heating in the solar-system history.

Phaethon shows spectroscopically bluer than the solar color, as against usual C-type spectroscopy generally being in neutral–red with the meteoritic analog of CI/CM chondrites. The visible (hereafter, VIS) to near infrared (hereafter, NIR) spectroscopic continuum of Phaethon indicates a negative slope of normalized gradient of reflectivity along with the UV/*B*-band falling-off and lacking the $0.7\text{-}\mu\text{m}$ absorption feature due to decomposition of phyllosilicates. Thus the asteroid is classified at the B/F-type taxonomy as well as Pallas by the VIS–NIR spectrophotometries (e.g., Tholen 1985; Luu & Jewitt 1990; Binzel et al. 2001; Licandro et al. 2007, and others), i.e., suggesting a dehydrated and metamorphosed C-type asteroid. In fact, Phaethon is a low-albedo asteroid, geometric albedo $pv = 0.122 \pm 0.008$ along with $D = 5.1 \pm 0.2$ km-size and relatively high thermal inertia $\Gamma = 600 \pm 200 \text{ J m}^{-2}\text{s}^{-1/2} \text{ K}^{-1}$ (Hanuš et al. 2016a,b) almost equivalent to Cold Bokkeveld (CM2) of $< 650 \text{ J m}^{-2}\text{s}^{-1/2} \text{ K}^{-1}$ (Opeil et al. 2010). These physical parameters are of typical B-type asteroids (Alí-Lagoa et al. 2013). However, a strikingly matching meteoritic (surface) analog for Phaethon has never been identified yet. Nevertheless, thermally metamorphosed CI/CM chondrites are the best candidate analog for the C/G/B/F-type asteroids (Hiroi et al. 1993, 1996), since those carbonaceous chondrites underwent thermal history of high-temperature heating at more than several 100 K and dehydration for a certain period of time after aqueous alteration in their parent bodies (Nakamura 2005, 2006; Nakato et al. 2008). Indeed, Phaethon’s sub-solar surface temperature of 800–1100 K at perihelion is obviously higher than the temperatures starting serpentine–phyllosilicate decomposition at ~ 573 K and dehydration at ~ 673 K (Akai 1992). Serpentine in carbonaceous chondrites

also show similar decomposition temperature of serpentine (Nozaki et al. 2006). Also, the temperatures starting saponite-phyllosilicate decomposition and dehydration are higher by ~ 200 K than those of serpentine-phyllosilicate (Nozaki et al. 2006). Major constituents of CI and CM chondrites are saponite-rich and serpentine-rich mineralogy in their fine-grained matrix-phyllosilicates, respectively. In addition, the reflectance spectra of CI/CM chondrites show bluer-slope in the case of their grains being coarser and larger than $100 \mu\text{m}$ -order in size (Cloutis et al. 2013), so-called, “grain size effects”. However, Clark et al. (2010) advocated CK chondrites being another candidate analog for Phaethon, comparing their VIS–NIR spectral shapes. Also, some Ureilites exhibit a blue spectral slope (Jenniskens et al. 2009; Cloutis et al. 2010), along with shallow Band I/II (of mafic iron silicate absorption band) features, although Band I/II features are generally not recognized in Phaethon’s spectrum. Besides, space-weathering effects should strongly influence on the C-type asteroid spectroscopy, which tends to be darker and bluer again (Moroz et al. 2004; Matsuoka et al. 2015). Dundon (2005) found a spectral similarity between Phaethon and carbon black in the VIS–NIR range. This makes us imagine that Phaethon’s surface is coated by some “carbonized” material produced by space-weathering (Moroz et al. 2004). Phaethon would have originally been holding Pallas’s surface and/or inner color, if Pallas is actually the parent body of Phaethon. However, the negative spectral slope of Phaethon is extremely steeper in the VIS-range by a factor of 40 than that of Pallas (Clark et al. 2010). In fact, Phaethon is known to be considerably bluer object than any other SSSB, according to Luu & Jewitt (1990) and Clark et al. (2010). The physical parameters of Phaethon are bound up by G. Hahn ¹.

Another hot topic worth noting is that Phaethon is indeed an active asteroid as categorized by rocky comet (Jewitt et al. 2015). Although no trace of Phaethon’s cometary

¹<http://earn.dlr.de/nea/003200.htm>

activities has been found yet by ground-based observations (e.g., Chamberlin et al. 1996; Urakawa et al. 2002; Hsieh & Jewitt 2005, and others), recurrent weak cometary activities were detected in 2009, 2010, 2012, and 2016 by the spaceborne coronagraphic observatory, the Heliospheric Imager, HI-1/SECCHI onboard NASA’s STEREO-A spacecraft (Jewitt & Li 2010; Li & Jewitt 2013; Jewitt et al. 2013; Hui & Li 2017). Then Phaethon’s brightness increased by ~ 2 magnitude (hereafter, mag) near its perihelion. The dust tail was also found in 2009, 2012, and 2016 whose β -syndyne indicated that released dust particles were in an effective radius of $\sim 1 \mu\text{m}$ -order: thus too small in size to replenish the Geminid meteoroid stream (Jewitt et al. 2013; Hui & Li 2017). Those activities may be induced by dust ejections due to thermal fracture and/or thermal decomposition of surface materials around perihelion (Li & Jewitt 2013; Jewitt et al. 2013). Especially, the north-pole (NP) region of Phaethon will be selectively and successively heated over 1000 K just after the perihelion passage, particularly due to non-rotational NEATM-like effect (Galushina et al. 2015), if we take Phaethon’s pole axis solution of Krugly et al. (2002) or Ansdell et al. (2014): both pole solutions were determined to be high-obliquity close to Phaethon’s orbital plane and the ecliptic plane. On the other hand, Hanuš et al. (2016a) very recently presented somewhat different pole axis solution with moderate-obliquity. This pole solution indicates that Phaethon’s entire surface has been almost equally burnt out by the solar radiation heating rather than selective and successive NP-region heating, because its pole orientation should be substantially moved by secular pole axis precession. If it is true, this may result in a saturation of the thermal metamorphism in Phaethon’s entire surface. Nevertheless, if the PGC members (hereafter, PGCs) were generated by any impact-induced splitting or breakup event on Phaethon (or PGC precursor), C-type-like surface, implying the primordial internal structure of Phaethon (or PGC precursor), may be still exposed somewhere on Phaethon’s surface. If so, this C-type-like surface materials possibly consist of water- and volatile-bearing CI/CM-like primitive carbonaceous

chondrites, which may contribute the cometary activity of Phaethon.

In fact, Phaethon is probably the main mass among the PGCs, whereas the second-largest mass candidate is an 1.3-km-sized object, Apollo-type NEA (155140) 2005 UD (Ohtsuka et al. 2006), which is also an NSA. Another large PGC candidate is Apollo-type NEA (225416) 1999 YC (Ohtsuka et al. 2008; Kasuga & Jewitt 2008), though its orbital energy, a^{-1} , is somewhat smaller than Phaethon and 2005 UD. The dynamical motion of 2005 UD shows comparable q - i oscillating Lidov–Kozai cycle with that of Phaethon, time-lagging by ~ 4600 yr (Ohtsuka et al. 2006). From broadband photometric measurements, the surface color of 2005 UD indicates that it is most likely to have the B/F-type taxonomy, compared with that of Phaethon (Jewitt & Hsieh 2006; Kinoshita et al. 2007; Kasuga & Jewitt 2008). The B/F-type asteroids are very rare, comprising only $\sim 5\%$, among all the classified NEAs (Jewitt & Hsieh 2006): thus, the probability that Phaethon and 2005 UD would be found by randomly drawing from all of the NEAs is extremely low. It is interesting that $\sim 1/4$ rotational part of 2005 UD shows a red-spectral slope, suggesting likely the C-type color (Kinoshita et al. 2007). Hence, this $\sim 1/4$ part may imply an exposition of the primordial internal structure of the PGC precursor by a splitting or breakup event, i.e., less-metamorphic and less space-weathered surface on 2005 UD. So, we hypothetically suspect that 2005 UD have arisen from the disintegration of Phaethon (or PGC precursor) ~ 1 Myr ago (Ohtsuka et al. 2006), a long time after Phaethon (or PGC precursor) being released from Pallas within 30 Myr ago, if the precursor actually attribute to Pallas. Then the PGCs would be generated, in which smaller decameter- and meter-sized bodies, far-smaller fragments and dusts may have been produced by power-law scaling. So, some decameter- and meter-sized PGC bodies may penetrate into the earth’s atmosphere with relatively high velocity of ~ 33 km sec $^{-1}$, when most of them should be highly ablated and thus not survive. However a little bit of these bodies may survive and be preserved on the Earth’s ground somewhere as the

Phaethon (or PGC) meteorites (Madiedo et al. 2013). The rest of fragments and dusts may generate the Geminid and Daytime Sextantid meteor streams and other PGC streams (Babadzhanov & Obrubov 1992; Ohtsuka et al. 1997). Also it is slightly possible that NEA 2011 XA₃ is an impactor or an interloper of the PGC (Urakawa et al. 2014).

If our working hypothetical scenario is true, some rotational part of Phaethon should show the neutral- to red-spectral slope as the C-type color as 2005 UD does. This should be a strong signature of the splitting or breakup event on Phaethon (or PGC precursor) in the past, and provide yet another strong piece of evidence for a common origin of Phaethon and 2005 UD. However, the (past) other works for the VIS(–NIR) spectroscopic observations of Phaethon have been carried out by single frame shot or so. Hence, the existence of the C-type color on Phaethon’s surface has been not well recognized, although a possible surface inhomogeneity was briefly discussed (Licandro et al. 2007; Ohtsuka et al. 2009).

Therefore, to ensure our hypothesis, we carried out time-series VIS spectroscopic observations of Phaethon in 30 November–2 December, 2007, covering more than one full rotational phase (or period $P \sim 3.6$ hr: e.g., Hanuš et al. 2016a), when the asteroid approached the Earth within ~ 0.2 AU and then brightened up to visual magnitude, $m_v \sim 13$ mag. Also, *R*-band photometric observations were simultaneously performed in order to complement our spectroscopy. Detail of our observation is described in Section 2. We present the results of our rotationally time-resolved VIS-spectrophotometries of Phaethon and give discussions about them in Section 3. Finally we summarize and conclude our works in Section 4.

2. Observations and Data reduction

2.1. Spectroscopy and its testing

The VIS spectroscopic observations of Phaethon were carried out by using the Lulin 1.0-m (One-meteor) Telescope (thus commonly called “LOT”) with a low-dispersion spectrograph named “Hiyoyu” at Lulin observatory operated by the Institute of Astronomy, National Central University. The observatory is located near the summit of Mt. Lulin (MPC Observatory code: D35, $120^{\circ}52'25''\text{E}$, $23^{\circ}28'7''\text{N}$, $H = 2862$ m above sea level) in the central region of Taiwan. The spectrograph, Hiyoyu, which means rainbow in the language of native Taiwanese of Tsou tribe, was mounted on the Cassegrain focus (F/8) of LOT and used for this study. Hiyoyu is almost identical to the Gunma Compact Spectrograph (GCS) at the Gunma Astronomical Observatory (Hamane et al. 2002). GCS was originally designed for F/12 of the Gunma telescope, so we attached a conversion lens to convert from F/8 into F/12 before feeding the light into Hiyoyu for using LOT. The focal lengths of the collimating optics and camera optics are 240 mm and 200 mm, respectively. The dispersion element is due to reflective gratings, which is replaceable for two modes for our instrument by selecting low resolution gratings of 300 gr mm^{-1} or 1200 gr mm^{-1} . Here we chose the grating of 300 gr mm^{-1} along with the 390×1.5 arcsec slit to record the spectral shape along with overall features of Phaethon in the VIS-range. This 1.5-arcsec slit is in fact narrow in width for the VIS-spectroscopic observations. However, since the seeing size of stellar FWHM (full width at half maximum) at Lulin observatory is generally within 1.5 arcsec, the 1.5-arcsec width slit is acceptable for majority of uses. We used the Apogee 1K-CCD camera, AP-8 (Kodak KAF-1001E), as a detector for spectral images, whose format having 1024×1024 pixels ($24 \mu\text{m pixel}^{-1}$). Thus CCD chip size is 24.6×24.6 mm, which results in pixel scale being $0.62 \text{ arcsec pixel}^{-1}$. Resultant spectral resolution $R(\lambda/\Delta\lambda)$ is ~ 330 (at $\lambda = 5000 \text{ \AA}$). The cooling temperature of the CCD is set to -50°C , and this is achieved by

both thermoelectric cooling and water circulation. The spectral wavelength ranges between 3800–7600 Å, covering over the VIS-range. The SBIG Astronomical Instruments CCD camera, ST-8, was used as a slit viewer monitoring camera, and was also used to adjust the telescope tracking manually during the exposures of Phaethon. Although LOT has a function to perform the differential tracking, our main target, Phaethon, was in fact a fast moving NEA that quickly approaches the Earth and thus fine-adjustment of manual tracking was important to obtain high quality spectra. The Fe-Ne-Ar hollow cathode lamp is used for the wavelength calibration. The specification of Hiyoyu ² is listed in Table 1.

In this way, the observations were made for three successive nights in 30 November–2 December in 2007. We continuously took a 300-sec integration in each exposure when Phaethon has good visibility in observation. Consequently, a total of 68 VIS-spectroscopic data of Phaethon were successfully recorded, which may cover more than one full rotational phase, among which 24, 27, and 17 data were obtained in each night, respectively. The log of the observations is summarized in Table 2. Then we selected HR1544 and HR3454 as the spectrophotometric standard stars, and HIP22349 and HIP46404 as the solar-analog G2V stars. Their images were generally recorded every 30-minutes interval between observations of Phaethon. Sometimes we observed the Moon as another solar-analog star for reference. The Fe-Ne-Ar lamp spectra were also obtained along with the exposures. The dark and dome flat-field frames were taken before and after the observations of each night.

All the spectral images were dark-subtracted and flat-fielded along the standard data reduction procedure using the image-analysis software package NOAO IRAF (Image Reduction and Analysis Facility). Extraction of the spectrum from two-dimensional spectral images, subtraction of the sky background, and wavelength and flux calibrations were carried out by using the `twodspec` and `onedspec` tasks in IRAF. After that, an asteroid

²for more detail, see http://www.lulin.ncu.edu.tw/lot/Hiyoyo_spectrograph_manual.pdf

spectrum was divided by the spectra of the G2V star, and finally we obtained a scaled reflectance of the asteroid.

Before observing Phaethon each night, we performed the VIS-spectroscopic observations for some bright main belt asteroids to test and confirm the instrument functionality, procedure of our observations, and subsequent calibration and data reduction process for Phaethon. Then we obtained the VIS-spectra of Main-belt S-type asteroid (548) Semiramis and F-type asteroid (704) Interamnia, as represent in Figure 1. Both the asteroid spectra using Hiyoyu show typical taxonomic features, respectively. The VIS-spectra of both the asteroids were in fact recorded by the SMASS II (Phase II of the Small Main-Belt Asteroid Spectroscopic Survey: Bus & Binzel 2002), which are superimposed in Figure 1 for comparison. The SMASS II works are well-known as building global reputation in the VIS-NIR spectroscopy of asteroids. The first goal of our study is to obtain and check out the overall flux curve and shapes of our VIS-spectra. As can be seen from Figure 1, the spectral flux curves for Semiramis and Interamnia, recorded by our Hiyoyu system, agree rather well with those by the SMASS II works. Hence, we can say that we have confirmed that the Hiyoyu system is safe to study the VIS-spectroscopy of the SSSBs.

2.2. Photometry

Simultaneous photometric observations for the target asteroid are important to complement our rotationally time-resolved spectroscopy. So, we can identify a rotational phase at the time for each spectrophotometry based on the rotational phase curve, i.e., lightcurve, constructed from time-series photometries. Such complementary photometric observations are carried out by using the 0.36-m Ritchey-Chretien (F/8) telescope at the Miyasaka observatory (MPC Observatory code: 366, $138^{\circ}17'50''$ E, $35^{\circ}51'57''$ N, H= 860 m above sea level) in Japan. Then the SBIG 1K-CCD camera, STL-1001E (Kodak

KAF-1001E), is used as a detector. This camera has 1024×1024 pixels ($24 \mu\text{m pixel}^{-1}$), thus the CCD chip size is 24.6×24.6 mm. So, the field of view (FOV) for the CCD chip is the square of $29'.4$ with a pixel scale of $1.72 \text{ arcsec pixel}^{-1}$. This is spatially well-sampled at the typical seeing size of stellar FWHM at the observatory, since, in winter season, the seeing conditions at observatories in east-Japan located near the coast of the Pacific ocean are generally not good. The stellar FWHMs are in fact $6\text{--}7$ arcsec during our photometries. The CCD is cooled by the thermoelectric cooling, and the operation temperature of the CCD was -35°C .

In such a manner, *R*-band photometric observations of Phaethon were performed on two nights, 30 November and 1 December, 2007, simultaneously with the VIS-spectroscopic observations at Lulin. We took continuously a 60-sec integration in each exposure on 30 November and on the first half on 1 December, and a 30-sec integration on the last half on 1 December in order to avoid the contamination due to a bright star in FOV. The angular velocity of Phaethon's sky motion was rather large in the RA (Right Ascension) direction, $6\text{--}7 \text{ arcsec min}^{-1}$, during our observations in Phaethon's close approach to Earth. It was comparable to the stellar FWHMs at the observatory, and it does not give a big impact to the photometry under the sidereal tracking for Phaethon. As a consequence, we acquired a total of 144 photometric data: 83 frames of photometric data in total during 4.7 hours on 30 November and 61 frames of those during 3.5 hours on 1 December, respectively. We also measured the flux of several Landolt's standard stars, which were imaged under almost the same air mass with Phaethon. All the photometric data were obtained through the Johnson-Cousins-based *R*-band filter. Dark and twilight flat-field frames were taken after the observations in each night.

All the photometric images were dark-subtracted and flat-fielded based on the standard CCD data reduction procedure using IRAF, too. Then the aperture photometry was done

using a circular aperture three times larger than the radial profile of Phaethon’s FWHM.

3. Results and Discussion

3.1. Time-variable spectra of Phaethon

Here we deal with the normalized spectral gradient of reflectivity in the VIS-range. Luu & Jewitt (1990) first reduced the spectral gradients of asteroids, fitting the linear-function of wavelength. This method is useful for the taxonomic classification of asteroids. Therefore, we applied this linear least-squares fit to Phaethon’s spectral slope and measured its spectral gradient for each frame. The normalized spectral gradient of reflectivity, S' (in unit of %/0.1 μm), in the wavelength range between λ_1 and λ_2 is defined by Luu & Jewitt (1990) as

$$S'(\lambda_1, \lambda_2) = \left(\frac{dS/d\lambda}{S_{\lambda_c}} \right), \quad (1)$$

where $dS/d\lambda$ is a changing rate of the reflectivity gradient in the range, $\lambda_1 = 0.45 \mu\text{m}$ and $\lambda_2 = 0.65 \mu\text{m}$ in our study. λ_c is the center of this wavelength range, so here we take $\lambda_c = 0.55 \mu\text{m}$. Thus $\lambda_1 \leq \lambda_c \leq \lambda_2$, and the spectral slope is represented nearly by the straight line in this interval. S' serves as a measure of the color of the asteroid, applying the solar color as a standard. Hence the color of the asteroid suggests red when $S' > 0$, as against blue when $S' < 0$. The VIS-region contains very limited information on reflectance properties for the S' -positive taxonomic classes, i.e., S- and C-types. However, we can easily discriminate whether or not it is B/F-type class, judging by the S' -value in the VIS-region, since the B/F-type taxonomic classes only exhibit the negative S' -values. Hence, here we specially propose calling an extremely blue-slope for Phaethon’s VIS-spectrum “Phaethon Blue”. This comes from the VIS-spectrum recorded by Luu & Jewitt (1990) on 6 October, 1988 (the spectrum LJ1988 in Table 5), and re-measured at $S' = -11$ by Licandro et al.

(2007). The S' -value of Phaethon is more effective and lower in the VIS-range than in the NIR-range, by the factor of 10 (Licandro et al. 2007). In fact, the blue-spectral slope of the B-types in the VIS-range shows negatively more precipitous than that in the NIR-range (Alí-Lagoa et al. 2013). Therefore, our time-series VIS-spectrophotometry may have more advantage in significantly distinguishing spectral flux (or color) variation of Phaethon, if any, than applying the NIR-spectroscopy.

The results of our Phaethon’s VIS-spectrophotometries for S' along with their ephemerides and geometric parameters are summarized in Table 3. The aspect angles (i.e., sub-Earth latitude on Phaethon), ϕ_K , ϕ_A , and ϕ_H , are calculated on the basis of the pole solution (SOL, hereafter) K by Krugly et al. (2002), SOL A by Ansdell et al. (2014), and SOL H by Hanuš et al. (2016a), respectively. Their pole axis parameters are presented in Table 4. Also, the time-series VIS-spectra of Phaethon are patched together in Figures 2, 3, and 4 for the 30 November, 1 and 2 December observations, respectively. All the spectra show mostly featureless, as pointed out by several works so far. The $0.7\text{-}\mu\text{m}$ absorption feature (due to Fe^{3+} abundance in phyllosilicates: Vilas & Gaffey 1989) was not visible in any of our spectroscopic data at all. Also, no cometary features were detected in our data, although Phaethon sometimes displays the cometary activity near perihelion. But, one of our most significant results in this work is that Phaethon spectroscopically shows time-variable and variety in the taxonomic classification, since Phaethon’s S' is diverse in the values from -11.45 ± 1.25 (so-called, Phaethon Blue) for the spectrum 1130-02 (midtime 30 November, 17:58:12 UT) to 6.63 ± 0.26 for 1202-05 (2 December, 18:41:53 UT). It roughly corresponds to the range between B- and C-(or Cb-)type colors in the Bus (1999) spectrometric taxonomy, suggesting there exists an inhomogeneous surface property on Phaethon, as we expected. Nevertheless, Phaethon’s surface seems to be dominantly covered with the B-type material, since a total of 53 out of 68 spectrophotometries, thus 78%, are in the negative S' -values, along with the UV/ B -band falling-off, as against the

rest 15 spectrophotometries, 22%, being in the positive ones, with a weak UV/*B*-band absorption feature, as seen in Table 3 and Figures 2–4. Therefore, the S' -values seem to be correlated with the UV/*B*-band feature strengths.

The S' -value diversity of our results is almost overlapped by assorted single frame shots of the other 15 VIS-spectrophotometries, ranging between –11 to 23, as compiled in Table 5. Among those, however the only one red-slope spectrum of Phaethon, CB1983 ($S' = 23$), has been recorded by Cochran & Barker (1984), i.e., 7% of 15 spectra, whether stochastically by chance or necessity.

Our time-series VIS-spectrophotometry reveals that S' alternately exhibits maximum and minimum with some periodicity, gradually changing. In fact, the red-slope spectra unevenly cluster at certain time regions, as shown in Table 3: only one spectrum (1130-11) on 30 November; 9 spectra (1201-09, 17, 18, 20, 21, 22, 25, 26, and 27) on 1 December; and 5 spectra (1202-01, 02, 03, 04, and 05) on 2 December. Therefore, we next carried out periodic analysis for the time-series VIS-spectrophotometries based on Phaethon’s rotation period in order to find whether or not red-colored region is located at the particular rotational phase. It may be involved with local (or longitudinal) specific materials and/or structure.

3.2. Revisit of Phaethon’s rotation period: $P \sim 3.6$ hours or ~ 7.2 hours?

Before examining the rotationally time-resolved spectroscopy, we revisit the axial rotation state of Phaethon. We also analyzed it using our *R*-band photometric data. The sidereal rotation period of Phaethon has been reported by several works so far. Meech et al. (1996) first reduced a “double-peaked” rotation period of $P = 3.604 \pm 0.0011$ hr based on the data acquired on three nights in December, 1994–January, 1995, from the UH88

telescope of IfA/UH (Institute for Astronomy, University of Hawaii) and from the Lowell observatory. Pravec et al. (1998) also obtained two $P \sim 3.6$ -hr lightcurves on 1 and 2 November, 1997 and in November–December, 2004³, respectively, from the Ondřejov observatory, who derived a synodic “single-peaked” lightcurve with $P = 3.57 \pm 0.02$ hr based on the 1997 data. It is somewhat “noisy” along with rather small amplitude, which implies that the lightcurve was possibly derived under near pole-on geometry. Krugly et al. (2002) obtained two $P \sim 3.6$ -hr lightcurves with small amplitude, using respectively 4-night data in September 1996 and 2-night data in November 1997, from the Chuguevskaya station, both of which show single-peaked ones, hence similar to that observed by Pravec et al. (1998). Then they determined the pole axis orientation, SOL K, as listed in Table 4, which is the first candidate between their two SOLs. Krugly et al. (2007) carried out photometric observations again in 2004, when they obtained $P = 3.6052 \pm 0.0008$ hr. Gaftonyuk et al. (2010) obtained $P = 3.604$ hr based on their photometries in 2004, 2006, and 2007 from the Crimean Astrophysical Observatory. Ansdell et al. (2014) reduced $P = 3.6032 \pm 0.0008$ hr based on 15-night photometric dataset in 1994–2014, observed by the IfA/UH team, whose lightcurve patterns show a mixture of single- and double-peaked “looking” ones on different nights, including the data obtained by Meech et al. (1996). They also solved the pole axis orientation, SOL A (see Table 4) and the lightcurve-inversion convex shape model. Warner (2015) found another $P \sim 3.6$ -hr double-peaked lightcurve from CS3-PDS, using 8-night data in November–December, 2014: his $P = 3.6039 \pm 0.0002$ hr. Most recently, Hanuš et al. (2016a) may have reached the top quality in analyzing Phaethon’s rotation state, who reduced $P = 3.603958 \pm 0.000002$ hr, using all the available photometric data of Phaethon over the world, including the IfA/UH dataset: the world’s biggest, 49(out of 51)-night dataset in the longest observational arc in 1994–2015. Consequently, they performed the

³the 2004 observations: <http://www.asu.cas.cz/~ppravec/newres.txt>

reconstruction of fine structure by long-term rotational phase curve fitting along with the pole axis determination, SOL H (see Table 4) and the convex shape model. Therefore, number of photometries (or nights) are in order of increasing as SOL K<A<H.

Hence, the previous works claim $P \sim 3.6$ hr for Phaethon. These rotational parameters are compiled in the Asteroid Lightcurve Data Base (LCDB) by B. D. Warner⁴, from which we can find that the lightcurve amplitude of Phaethon distributes over 0.07–0.34 mag.

After differential photometry using our R -band images, we performed the periodicity analysis, applying the Period Searching & Light Curve Fitting Program software “cyclocode”⁵ developed by Dermawan (2004), which is an implementation of the Lomb periodogram. As a result, we found the sidereal rotation period of Phaethon to be $P = 3.6024 \pm 0.0130$ hr based on the best fitted single-peaked lightcurve. Also, we got a similar result using the Python module, “astroML”, for machine learning and data mining for astronomy⁶. It perfectly matches with those previously reduced as above, especially the reduction of Hanuš et al. (2016a) being within the 1σ -level of our reduction. By phase-folding with $P = 3.6024 \pm 0.0130$ hr, we obtained the single-peaked synthetic lightcurve, as plotted in Figure 5(a). The RMS residuals of the fitted lightcurve seem to be somewhat larger and noisy like the other single-peaked lightcurves obtained by Pravec et al. (1998) and by Krugly et al. (2002). Asteroids as 3D-triaxial ellipsoid bodies usually describe a double-peaked phase curve in one full rotation, whereas a single-peaked phase curve may uncommonly occur when the body shows bidimensionally near round shape at near pole-on geometry to the Earth (e.g., Zappalà 1980; Kaasalainen et al. 2005). Therefore, we examined the possibility whether or not sub-Earth latitude on Phaethon was near pole-on

⁴<http://www.minorplanet.info/lcdbquery.html>

⁵e.g., available at <http://www.toybox.rgr.jp/mp366/lightcurve/cyclocode/cyclocode.html>

⁶<http://www.astroml.org/>

situation during our observations. Three geometric models of Phaethon as viewed from the Earth at the time of 19:35:50 UT, 1 December, at which the spectrum 1201-17 was recorded, i.e., near median time of our spectroscopic observations, are schematically illustrated in Figure 6(a)–(c), assuming the asteroid to be a spherical body. They were reconstructed from SOLs K, A and H, when their aspect angles were $40^\circ.6S$, $26^\circ.3S$, and $61^\circ.7S$, respectively. These aspects are calculated as seen from the geocenter, but the parallax of the geocenter with the Lulin observatory is tiny and negligible. The phase angle, α , was $61^\circ.90$, thus the ratio of the luminous area to the total area of disk, $k = 0.5(1 + \cos \alpha) = 0.74$. If we define Phaethon’s north-pole orientation as the sunlit side at the perihelion, the southern hemisphere faces to the Earth at the time of observation in every models. Then SOL H exhibits a retrograde rotation against SOLs K and A. During the photometric observations, α changed a little from $58^\circ.87$ to $61^\circ.81$, and likewise ϕ_K , ϕ_A , and ϕ_H changing from $43^\circ.5S$ to $40^\circ.5S$, $29^\circ.1S$ to $26^\circ.2S$, and $61^\circ.9S$ to $61^\circ.7S$, respectively. They do not so strongly affect the RMS residuals of phase curves in our photometries. Therefore, Phaethon did not situate in near pole-on viewing geometry in either SOL case and its single-peaked lightcurve would be unexpected from our observations.

On that account, by phase-folding with $2P$, we obtained the double-peaked synthetic lightcurve with the period of 7.2048 ± 0.0820 hr, as given in Figure 5(b). The double-peaked lightcurve visually exhibits a better fitting than the single-peaked one, as customary practices, although the 1σ -error of ± 0.0820 for this $2P$ phase-folding is larger than that of ± 0.0130 for the $P \sim 3.6$ -hr phase-folding. In addition, photometric data points of the $2P$ phase-folding have $\sim 15\%$ coverage gaps in its full rotational phase, as another disadvantage. Nevertheless, significant differences between the first- and second-cycle patterns and between their amplitudes arise in this $2P$ phase-folding, double-peaked lightcurve, which denies a possibility of the single-peaked lightcurve solution against Phaethon. Hence, these observational facts suggest that $P \sim 7.2$ hr is more preferable for

Phaethon than ~ 3.6 hr along our reduction. Then the lower limit of the axis ratio of Phaethon during the photometric observations is estimated from the lightcurve amplitude, assuming that the variability comes entirely from the elongated shape of the object. The lightcurve amplitude for R -band magnitude, Δm_R , is ~ 0.22 mag, near the median among LCDB for Phaethon. This implies the lower limit of the axis ratio of 1.22 from the relation

$$\frac{a}{b} > 10^{0.4\Delta m_R}, \quad (2)$$

where a/b is the axis ratio of primary and secondary axes. This near round shape profile was supported by the Arecibo radar observation targeted Phaethon that was operated one-week later of our observations in 2007 (Lance Benner 2016, personal communication). A similar tendency is supported by the convex shape derived by Ansdell et al. (2014) and Hanuš et al. (2016a) based on $P \sim 3.6$ hr. Both the rotation periods of $P \sim 3.6$ hr and ~ 7.2 hr do not make any difference in the pole axis determination, while they should make a big difference in the shape modeling. The $P \sim 3.6$ -hr double-peaked-look lightcurve, detected by previous works, may be caused by Phaethon's partially-angular outline.

Likewise the sidereal rotation period of 2005 UD based on the best fitted single-peaked lightcurve was reduced at $P \sim 2.62$ hr, thus double the obtained periodicity, $P \sim 5.24$ hr, should be the actual one (Jewitt & Hsieh 2006; Kinoshita et al. 2007). In fact, it would be natural that a larger body spins at lower rotation rate than smaller fragmentary bodies do among identifiable asteroid family members (e.g., Fujiwara & Tsukamoto 1981; Kadono et al. 2009). Therefore, the rotation periods of Phaethon's ~ 7.2 hr and 2005 UD's ~ 5.2 hr match up well with the size relation between Phaethon and 2005 UD: the 5.1 km-size main mass and the 1.3 km-size secondary mass among the PGCs, respectively.

3.3. Rotational phase variation of the spectral gradients, S'

We finally verify the presence or absence of some correlation between spectral gradients of Phaethon and its rotational phase by phase-folding with $P = 3.6024$ hr and with 7.2048 hr. They are presented in Figure 7(a) and (b), where a total of 68 S' -data points are plotted on the rotational phase by phase-folding with $P = 3.6024$ hr for panel (a) and with $P = 7.2048$ hr for (b). When we draw a comparison about them, the spectral gradients seem to be almost randomly scattered in panel (a), while surprisingly smoother changing in (b). Panel (a), by phase-folding with $P = 3.6024$ hr, seems to have a very weak trend of correlation between spectral gradients and rotational phase, whose S' -data points reach the maximum around the rotational phase ~ 0.5 and a minimum around ~ 0 or ~ 1 . On the other hand, panel (b) by the phase-folding with $P = 7.2048$ hr obviously reveals rather strong trend of correlation between those. The S' -data points gradually increase from the rotational phase around 0–0.1 as the minimum, and reach the maximum around the phase ~ 0.7 , after which it decreases markedly toward the phase ~ 1 of the minimum again. Thus this curve shows an asymmetric pattern. In addition, it is sure that a possible RMS residual for the S' -data points in panel (b) seems to be within almost a half of that in (a). Also, in any case of $P = 3.6024$ hr or 7.2048 hr, the S' -values in $\sim 30\%$ of the rotational phase seem to be in the positive zone, centered on the rotational phases ~ 0.5 and ~ 0.7 , respectively. Hence, we could successfully acquire rotationally-resolved spectroscopic data of Phaethon, of which particular rotational phase in fact shows a red-spectral slope as the C-type color, as well as 2005 UD, as we expected. We also ascertain that Phaethon's rotation period of $P = 7.2048$ hr is more preferable again, in which we observed $\sim 85\%$ of its full rotational phase of the S' -data points with $\sim 15\%$ coverage gaps.

Assuming Phaethon's rotation period of $P = 7.2048$ hr as correct, now we discuss a possible implication of smooth variation of the S' -values for Phaethon's spectral gradients

in Figure 7(b). It is natural to infer that the variation of the spectral gradients is caused by a longitudinal inhomogeneity rather than a latitudinal one on Phaethon’s surface, although Ohtsuka et al. (2009) expected the latitude-dependent color variations on Phaethon based on SOL K of Krugly et al. (2002).

If the solar-radiation heating is the main determining factor for Phaethon Blue and then SOL K is true, the solar-radiation heating effects on Phaethon may be a function of the latitude (Ohtsuka et al. 2009), since Phaethon was then regarded as having a highly-tilted pole axis and thus its mean precession rate can be negligible. These make Phaethon’s pole orientation to be almost fixed and stable against the ecliptic plane for the long term. Moreover, Phaethon’s orbital motion evolves slowly under the secular perturbation, mainly driven by the Lidov–Kozai circulation (Urakawa et al. 2014). Thus, the northern hemisphere would be selectively heated up to the temperature at 800–1100 K level near perihelion. Contrary, then the southern hemisphere may be heated to lower temperature at 600–800 K at most, thus barely exceeding the serpentine–phyllosilicate decomposition and dehydration temperatures at 573 K and 673 K, respectively. If so, the southern hemisphere may suffer a lesser degree of metamorphism than the northern hemisphere. However, we cannot find such a tendency from other spectrophotometric works (in Table 5) along with our works. In addition, we have recorded Phaethon Blue, $S' = -11.45 \pm 1.25$ for the spectrum 1130-02, despite the southern hemisphere dominantly facing to the Earth (then $\phi_K = 43^\circ.21S$), which is bluer than any other spectrophotometry for Phaethon and B/F-type asteroid, and comparable with $S' = -11$ for the spectrum LJ1988 (Luu & Jewitt 1990), previously the bluest record for Phaethon. Then LJ1988 was observed when the southern hemisphere facing to the Earth again, and when $\phi_K = 53^\circ.8S$. The spectrophotometries for CB1983, Ch1993, and Li2003 (see Table 5), recorded when facing the northern hemisphere to the Earth, obviously manifest that the northern hemispheric surface of Phaethon is not always bluer than Phaethon Blue. This discrepancy will be little change if we apply

SOL A of Ansdell et al. (2014), since the spin axes of SOLs K and A trend in almost the same direction each other. It should be, however, noted that Ansdell et al. (2014) found a possible latitude-dependent color variation on Phaethon from their multi-color photometric data.

On the other hand, if we take SOL H, things are largely different from those taking SOLs K and A. In fact, Hanuš et al. (2016a) speculated that SOLs K and A were incorrectly determined, since Phaethon’s surface color do not exhibits a latitude-dependent variation (Ohtsuka et al. 2009). From this background, they reduced another preferential pole solution, SOL H, using larger photometric dataset in longer photometric arc than SOLs K and A, mentioned above. In fact, its error circle is the least estimated at $\pm 5^\circ$ among three SOLs, and we may regard SOL H as the most reliable one. Hanuš et al. (2016a) demonstrated that their pole orientation should be highly changed by secular pole axis precession and the southern hemisphere is also preferentially heated by solar radiation heating around perihelion at present evolutionary epoch. If so, the entire surface, including the southern hemisphere, has long been almost equally burnt out by the solar radiation heating effects until now, which may saturate the thermal metamorphism in Phaethon’s entire surface, and also equally space-weathered, making Phaethon Blue. Therefore, there are no latitude-dependent variations on Phaethon, according to SOL H. If it is true, there never exists primitive chondritic materials on Phaethon’s entire surface, except for an exposition of likely primordial internal structure due to a large-scale splitting or breakup event long ago on Phaethon (or PGC precursor).

The aspect angles, $\phi_H = 61^\circ.02S\text{--}61^\circ.86S$, in our observations, have ever been in fact at the highest range in Phaethon’s southern hemisphere among all the VIS-spectroscopic observations, which maybe a special case. The spectrum La1994 recorded $S' = -3.9$ under the second-highest aspect, $\phi_H = 40^\circ.3S$ (Lazzarin et al. 1996), as listed in Table 5,

however normal color as Phaethon. Note that the only one red-slope spectrum, CB1983 with $S' = 23$, was obtained under $\phi_H = 16^\circ.3N.$, the second-highest northern-hemispheric latitude, maybe another special case.

3.4. Color composition on Phaethon's surface with C-type red-colored area

As we have seen, we detected only two spectra with $S' < -10$: 1130-02 (Phaethon Blue) and 1201-02 with $S' = -10.26$. Next, we consider the color composition in Phaethon's surface. Let us imagine that there are two distinct areas with two extreme pure colors on Phaethon's surface, i.e, Phaethon Blue and the C-type red color. Here we define two spectral gradients for their original colors as S'_B and S'_R , respectively. Then we can presume the observed (apparent) spectral gradient, S'_O , composed by the mixture of both colors with the area ratio ($A_1 : A_2$) between S'_B (for A_1) and S'_R (for A_2), as

$$S'_O \sim f(\alpha) \left(\frac{A_1 S'_B + A_2 S'_R}{A_1 + A_2} \right), \quad (3)$$

where $f(\alpha)$ is the phase reddening function, $f(\alpha) \sim 1$ when $\alpha > 40^\circ$ (Luu & Jewitt 1990), although $f(\alpha)$ for the C-complex asteroids has been not well-studied yet. Assuming S'_B and S'_R to be two extreme color-slopes for Phaethon ever recorded, -11 and 23 , we can reconstruct $S'_O \sim 5$, i.e., the S' -maximum among our spectrophotometries, such as at the rotational phase around 0.7 in Figure 7(b). Consequently, the red-colored area needs at least involving $\sim 45\%$ of Phaethon's luminous area, which results in at least 33% of Phaethon's disk, suggesting the red area to be ~ 2.9 km in diameter. This is considerably larger than 2005 UD's cross-section area (of 1.3 km in diameter), as illustrated in Figure 8. If we assume $S'_R \sim 5$, the red area needs 100% of Phaethon's luminous area and thus at least 74% of Phaethon's disk. Therefore, the larger S'_R is, the smaller the red area becomes, according to Equation (3). In any case, there exists a certain large C-type red-colored area somewhere, maybe mid-latitude in Phaethon's southern hemisphere, while Phaethon's

surface would be dominantly covered by the B-type-colored (or Phaethon Blue) material, suggesting thermally metamorphosed CI/CM chondrites. A part of the red area might be always face-on to the Earth during our VIS-spectroscopic observations, possibly including the SP region. The asymmetric S' -variation pattern, shown in Figure 7(b), would be due to disappearance of the red area under the sun-shadow and/or due to a non-circular asymmetric shape of the red area.

The petrogenesis for the C-type red-colored area may be due to a impact-excavation on Phaethon (or PGC precursor) with the splitting or breakup event that happened long time ago, when a large amount of PGCs would be released to the cosmic space, exceeding the mass of 2005 UD. Or contraction cracking due to repeated solar radiation heating >1000 K near perihelion may have triggered a splitting or breakup event on Phaethon (Granvik et al. 2016). Therefore, Phaethon’s surface and/or subsurface should be easily decomposed due to high-temperature heating (Akai 1992; Delbo et al. 2014), e.g. shock and solar-radiation heating effects, which may produce larger C-type area than we supposed. CI and CM chondrites are generally more friable and crumble than any other meteorite type, including CK chondrites (e.g., Tomeoka et al. 2003). In addition, it is likely that regolith grains are released from the C-type red-colored area as cometary dusts: matrix-phyllosilicate grains of CI/CM chondrites are in μm -order in size, thus well matching with the β -syndyne dust particles released from Phaethon. On the other hand, regolith grains in the Phaethon Blue area would aggregate by partially “unglazed”-like sintering effect with increasing heating time at subsolidus temperature of silicates; thus growing from fine to coarse grains. However, if we take $S'_R \sim 23$, then the red area will be fairly red, and thus may not be of the C-types: Cochran & Barker (1984) has indeed classified Phaethon as S-type on the basis of its relatively high S' -value. Therefore, our another scenario is that the red area consists of an ejecta blanket of the S-type impactor: in that case NEA 2011 XA₃ may be a remnant (Urakawa et al. 2014). If $S'_R \sim 5$, we may regard it to be still in the C-type taxonomy.

If we assume that the center of the red-colored area is located on the latitude of 45°S, as shown by Figure 8, we realize on the basis of SOL H that this area maximally absorbs heat energy from the Sun at 1.03 day before the perihelion passage of Phaethon. It is interesting that this is almost consistent with the dust-tail forming timescale of ~ 1 day just before the perihelion (Jewitt et al. 2013; Hui & Li 2017). Then the local equilibrium surface temperature at 45°S will be estimated to reach near maximum at 740–1000 K based on the FRM and NEATM, suggesting the temperature high enough for saponite and serpentine decomposition and dehydration. Hence, this may trigger thermal fracture in the red area, from which ~ 1 μm -order radius dusts release. In addition, the surface materials even in the red area would never be a water-reservoir due to periodic solar radiation heating. In fact, no 0.7- μm absorption feature was visible in any of our spectroscopic data, probably due to thermal-decomposition of Fe-bearing phyllosilicates as mentioned above. The S' -values of all the other spectrophotometries, listed in Table 5, may also be reconstructed by the mixture of the Phaethon Blue and the red-colored areas. A redness degree of the red-colored area would change into neutral–blue with time in the future, if the area is not an ejecta blanket of the S-type impactor.

3.5. Meteoritic analog for Phaethon

Here we discuss on the meteoritic analog and the petrogenesis of Phaethon’s surface blue-color (or Phaethon Blue). Ohtsuka et al. (2009) proposed that CI/CM chondrites heated at high- temperature may be the candidate analog for Phaethon’s surface. Recently, CK chondrites are suggested as another meteoritic analog candidate for Phaethon (Clark et al. 2010; Hanuš et al. 2016b). CKs are also thermally metamorphosed at high- temperature ranging 550–1270 K (Chaumard et al. 2012), which have undergone internal heating since CKs are supposed to come from the area near central core of the CV-CK clan

modeled parent body (Greenwood et al. 2010). In terms of the asteroid taxonomy, CV/CK chondrites would be originated from the K-type Eos collisional family (Mothé-Diniz et al. 2008; Greenwood et al. 2010). CK chondrites generally exhibit a blue-slope in the VIS-NIR range, whereas CV chondrites, located on more exterior–surface part of the modeled parent body, exhibit a red-slope (Cloutis et al. 2012b,a). Hence, it is possible that Phaethon’s surface is covered by the CV/CK-related materials. Space-weathering effects on CK-chondritic bodies have never been known yet.

For searching Phaethon’s meteoritic analog, we focus on the UV/*B*-band absorption feature which is very weakly seen in our VIS-spectrophotometric data. This feature presumably comes from the decomposition of Fe-bearing phyllosilicates in CI, CM, and CR chondrites as well as the 0.7- μ m feature (Vilas & Gaffey 1989). Generally, the UV/*B*-band falling-off works in conjunction with the less remarkable 0.7- and 3- μ m features with increasing the heating temperature (Hiroi et al. 1996). So, we measured the spectral gradients, S' , in the VIS-spectra of metamorphic carbonaceous chondrite samples through Equation (1): e.g. CI/CM anomalous chondrites underwent high-temperature heating, experimentally heated CI/CM chondrites, and CK chondrites, in various grain-sizes. Also, we picked up several CM chondrites for reference to confirm the grain size effect. These data are available by the Keck/NASA RELAB multi-user spectroscopy facility ⁷. The results of the S' -measurements are presented in Table 6, where we can see that only three spectra seem blue: Yamato (Y)-82162 (CI-an) chip is the only one natural meteorite that has a blue-slope with $S' = -0.32$. Nakamura (2005) classified this metamorphic chondrite at his heating stage **III** (heated at $< 750^\circ\text{C}$). The experimentally-heated Ivuna (CI1) at 700°C in the grain size $< 125 \mu\text{m}$ has the bluest-color among all, $S' = -4.24$. The experimentally-heated Murchison (CM2) at 900°C in $63\text{--}125 \mu\text{m}$ also shows a blue-slope

⁷<http://www.planetary.brown.edu/relab/>

with $S' = -0.98$, as against the meteorite in $< 63 \mu\text{m}$ showing a red-slope with $S' = 0.26$. The principal difference between those S' -values is probably due to the grain size effect. Belgica (B-)7904 and Y-86720 are CM anomalous chondrites that experienced intense heating and dehydration, both of which are categorized at Nakamura's heating stage IV ($> 700^\circ\text{C}$). However, they never exhibit a blue-slope in the VIS-range. It is interesting that PCA02012 (CM2) exhibits the reddest-slope, $S' = 28.85$, almost comparable to Phaethon's spectrum, CB1983 ($S' = 23$), which may also indicate a C-type red-color, rather than S-type. No CK chondrite has a negative S' -value ($S' = 0.34\text{--}7.29$) due to relatively strong UV/*B*-band absorption feature, since the CK-matrices never contain phyllosilicates. In addition, CK chondrites in fact show a strong silicate absorption feature of olivine at around $1.05 \mu\text{m}$, because well-crystalline olivine is a major phase of CKs (Cloutis et al. 2012a). But, either Phaethon and metamorphosed CI/CM chondrites do not possess this feature (Licandro et al. 2007). The S' -values for the RELAB CV and CO chondrite samples range in 3–8 and 10–20, respectively. The grain size effects are obviously recognized on all samples, as shown in Table 6. We summarized S' and several absorption features of Phaethon and of metamorphic chondrites as meteoritic analog candidates for Phaethon in Table 7. Based on matching the absorption features between them, we speculate thermally metamorphosed CI/CM chondrites as likely candidate meteoritic analogs for Phaethon. Especially, the heated Ivuna at 700°C in $< 125 \mu\text{m}$ deserves to be the top candidate analog among all the RELAB samples.

Nevertheless, there exists considerable gap in the S' -values between Phaethon Blue and metamorphosed CI/CM samples. $S' \sim -11$ for Phaethon Blue has not been reproduced by the RELAB spectroscopic experiments yet. Phaethon would be the most metamorphic C-complex asteroid in our solar system, along with heavily space-weathered in the near-Sun environment. Consequently, Phaethon Blue became the most extreme blue among the SSSBs. Having Pallas' surface and/or subsurface color as the initial condition, Phaethon

Blue may be created through additive color processes due to several combined effects, such as:

- Short-duration (shock) heating effect—Phaethon may be split and broken up by an impact event, around which surface materials would be highly metamorphosed.
- Long-duration heating effect—Phaethon should be recurrently heated at ~ 1000 K around its perihelion.
- Grain size effects—Phaethon’s surface may be covered by regolith grains larger than $100 \mu\text{m}$ -order size.
- Space-weathering—the fluxes of solar wind and micrometeorite bombardments increases as the asteroid approaches the Sun (Mann et al. 2004).

Those processes should substantially change Phaethon’s surface color, darker and bluer with time. Hence, we consider that Phaethon Blue may be the saturated color not only by thermal metamorphism but also space-weathering along with the grain size effects due to regolith grains $>100 \mu\text{m}$. We may be able to replicate Phaethon Blue using CI chondrites by laboratory experiments.

Note that the short-duration shock heating under high-pressure may induce a incipient partial melting process. This will make achondritic materials around the impact area, if PGCs were of impact origin (Arai et al. 2012).

3.6. Future opportunity to observe Phaethon: in 2017

As discussed above for our results, several open questions still remain concerning Phaethon’s nature. Further ground-based observations will give us some hints for these

questions. Especially, we have a good opportunity to confirm those during Phaethon’s next close approach to the Earth in 2017. Then Phaethon will flyby the Earth by minimum geocentric distance of 0.0689 AU with relative velocity of 31.9 km sec^{-1} on 16 December, around which Phaethon will be brighten up to $m_v \sim 10.7$ mag. Here we estimated the ephemerides of ϕ_H in 2017, whose time-variation is plotted in Figure 9, in which the observing conditions at solar elongation of over 90° turn up. Phaethon will be $m_v < 15.0$ mag in 22 November–18 December, thus providing good observing conditions for Phaethon’s spectrophotometry using the 2-m class telescopes. The minimum (=highest aspect) ϕ_H will reach down to 49.7°S on 21 November (marked by the red circle in Figure 9), in which the difference of ϕ_H with our VIS-spectroscopic observations in 2007 is only $\sim 12^\circ$. Incidentally, then ϕ_K and ϕ_A will be $64^\circ.4\text{S}$ and $51^\circ.7\text{S}$, respectively, thus also locating near mid–high latitude in the southern hemisphere. So, Phaethon will be observable in several days around 21 November, 2017 under similar geometric condition with the 2007 observations, when our hypothesis that there exists the large c-type red-colored area in Phaethon’s southern hemisphere could be tested by another VIS-spectroscopy. ϕ_H will rapidly change from the southern to northern hemisphere around Phaethon’s close approach to the Earth. Therefore, it is important for constraining the size of the red area to measure Phaethon’s S' by the VIS-spectroscopy under different aspect angles..

Furthermore, *in-situ* observations of Phaethon by a space mission should be by far the best way to elucidate what we have questioned. Several scientific mission proposals to Phaethon have been suggested so far (e.g., Belton & A’Hearn 1999; Kasuga et al. 2006). In fact, now Phaethon is selected as one of the top priority candidates for the JAXA DESTINY+ (Demonstration and Experiment of Space Technology for INterplanetary voYage) mission target object ⁸. The space mission that dispatches the DESTINY+

⁸<https://www.lpl.arizona.edu/jaxaworkshop/>

spacecraft and makes it flyby Phaethon near its descending node with relative velocity of 33–34 km sec^{−1} has already been designed by Sarli et al. (2015). This spacecraft is planned to have an onboard telescopic and multi-band cameras and also a dust analyzer. If the DESTINY+ mission is successfully achieved, it will make almost all of our questions on Phaethon answered. It will also serve as a complement of the OSIRIS-REx sample return mission that targets another B-type NEA (101955) Bennu (Lauretta et al. 2015)⁹. However, we should sufficiently acquire physical, geological, mineralogical, and dynamical information on Phaethon from further ground-based observations prior to the DESTINY+ mission.

4. Summary and Conclusion

We hypothesize that if the PGCs were generated by any splitting or breakup event on Phaethon (or PGC precursor), the C-type-like surface, implying the primordial internal structure of the precursor, may still expose somewhere in Phaethon’s surface after impact excavation. If it is true, some rotational part of Phaethon should exhibit the red-spectral slope as the C-type color as well as another large PGC candidate, 2005 UD. To ensure this working hypothesis, we carried out the time-series VIS-spectroscopic observations of Phaethon in 30 November–2 December, 2007, along with the *R*-band photometric observations, covering more than one full rotational phase, during which we recorded 68 VIS-spectra and 144 *R*-band photometric data. All the spectra show mostly featureless. But they show obviously time-variable and variety in the taxonomic classification, of which spectral gradients diverse between -11.45 ± 1.25 (so-called, Phaethon Blue, which is bluer than any other SSSB) and 6.63 ± 0.26 , thus ranging between B- and C-(or Cb-)type colors—

⁹see also <http://www.asteroidmission.org/>

an inhomogeneous surface property on Phaethon as expected. The S' -value diversity of our results is almost overlapped by assorted single frame shots of the (past) other VIS-spectrophotometries, ranging between -11 to 23 .

To find whether or not red-colored region is located at the particular rotational phase, we next carried out periodic analysis for our time-series spectra, applying our reduced rotation periods of Phaethon. Based on our photometries, a single-peaked sidereal rotation period of Phaethon was found to be $P \sim 3.6$ hr as pointed out by previous works: our $P = 3.6024 \pm 0.0130$ hr. However, we reduced another rotation period, $P = 7.2048 \pm 0.0820$ hr, by the double-peaked lightcurve fitting, which seems more preferable solution. The reason is then we did not observe Phaethon under near pole-on situation if according to either of the pole solutions, SOLs K, A, and H.

We verify the presence or absence of some correlation between spectral gradients of Phaethon and its rotational phase by phase-folding with $P = 3.6024$ hr and 7.2048 hr. We found a very weak trend of correlation between spectral gradients and rotational phase by phase-folding with $P = 3.6024$ hr, as against revealing rather strong trend of correlation by phase-folding with $P = 7.2048$ hr. Hence, here we ascertain again that $P = 7.2048$ hr is more preferable rotation period for Phaethon. In any of these cases, we successfully acquire rotationally time-resolved spectroscopic data of Phaethon, of which particular rotational phase shows a red-spectral slope as the C-type color, as 2005 UD dose, suggesting longitudinal inhomogeneity on Phaethon's surface.

If the solar-radiation heating is the main determining factor for Phaethon Blue and then SOL H that we regard as the most reliable pole solution is true, Phaethon's entire surface has long been almost equally burnt out by solar radiation heating until now. This may result in a saturation of the thermal metamorphism in Phaethon's entire surface, and also equally space-weathered, causing Phaethon Blue. However, we detected only two spectra

having $S' < -10$ among all, including one Phaethon Blue. Therefore, we next consider the color composition for Phaethon’s surface color. If we assume Phaethon’s surface is simply covered by two distinct areas with two extreme pure colors, i.e, Phaethon Blue and the C-type red color, we can presume and reconstruct the observed (or apparent) spectral gradient. As a result, we conjecture that the C-type red-colored area is considerably larger than 2005 UD’s cross-section area (~ 1.3 km), suggesting the PGCs have an impact-induced origin.

We also surveyed the meteoritic analog of Phaethon’s surface blue-color and found thermally metamorphosed CI/CM chondrites to be likely candidates. However, there exists considerable gap between the S' -values of Phaethon Blue and metamorphosed CI/CM samples. Hence, we consider that Phaethon Blue may be the saturated color not only by thermal metamorphism but also space-weathering along with the grain size effects due to regolith grains $>100 \mu\text{m}$.

We will have a good opportunity to confirm our VIS-spectrophotometric results during Phaethon’s next close approach to the Earth in 2017. Phaethon will be observable in several days around 21 November, 2017 under the similar aspect condition with our VIS-spectroscopic observations in 2007. At this opportunity, our hypothesis can be tested through the spectroscopy, and we will eventually know whether or not there is the large C-type red-colored area in Phaethon’s southern hemisphere.

Acknowledgement

A major part of our observations was carried out at Lulin Observatory operated by National Central University (NCU), Taiwan. The authors are grateful to the local supporters at Lulin: Jing-Chuan Du, Hao-Wei Shih, Jun-Shiung Shih, and Zong-Jing Wan.

A part of the data analysis was carried out at Center for Computational Astrophysics (CfCA), National Astronomical Observatory of Japan (NAOJ). Several spectroscopic data of Phaethon utilized here were obtained and made available by the MIT–UH–IRTF Joint Campaign for NEO Reconnaissance. Takahiro Hiroi gave us useful information on the spectroscopic data of carbonaceous chondrites, available by the Keck/NASA RELAB multi-user spectroscopy facility at Brown University. Alessondra Springmann introduced Lance Benner to us, who provided us with critical information on his unpublished radar observation in 2007 that gave us important clues for estimating the shape of Phaethon. The authors have benefited from stimulating enlightenment through discussions with Tomohiko Sekiguchi, Masateru Ishiguro, Fumi Yoshida, and Sunao Hasegawa. DK thanks Center for Planetary Science (CPS), Kobe University, for providing us with opportunities of interaction and discussion with number of planetary scientists. This work is supported by the research grant from National Science Council of Taiwan (ID 99–2112–M–008–013), the Ministry of Education of Taiwan under “Aim for Top University Program,” and the Kakenhi Grant of Japan Society for the Promotion of Science (JSPS), JP25400458/2013–2016 and JP16K05546/2016–2018.

REFERENCES

- Akai, J. 1992, Sixteenth Symposium on Antarctic Meteorites. Proceedings of the NIPR Symposium, 5, 120
- Alí-Lagoa, V., de León, J., Licandro, J., et al. 2013, *A&A*, 554, A71
- Ansdel, M., Meech, K. J., Hainaut, O., et al. 2014, *ApJ*, 793, 50
- Arai, T., Kasuga, T., & Ohtsuka, K. 2012, *LPI Contributions*, 1667, 6220
- Babadzhanov, P. B., & Obrubov, Yu. V. 1992, *Celest. Mech. Dyn. Astron.*, 54, 111
- Belton, M. J. S., & A'Hearn, M. F. 1999, *Adv. Space Res.*, 24, 1167
- Binzel, R. P., Harris, A. W., Bus, S. J., & Burbine, T. H. 2001, *Icarus*, 151, 139
- Binzel, R. P., Rivkin, A. S., Stuart, J. S., et al. 2004, *Icarus*, 170, 259
- Bus, S. J. 1999, PhD thesis, Massachusetts Institute of Technology, pp. 367
- Bus, S. J., & Binzel, R. P. 2002, *Icarus*, 158, 106
- Chamberlin, A. B., McFadden, L.-A., Schulz, R., Schleicher, D. G., & Bus, S. J. 1996, *Icarus*, 119, 173
- Chaumard, N., Devouard, B., Delbo, M., Provost, A., & Zanda, B. 2012, *Icarus*, 220, 65
- Clark, B. E., Ziffer, J., Nesvorný, D., et al. 2010, *J. Geophys. Res.*, 115, E06005
- Cloutis, E. A., Hudon, P., Hiroi, T., & Gaffey, M. J. 2012a, *Icarus*, 221, 911
- Cloutis, E. A., Hudon, P., Hiroi, T., et al. 2013, *LPI Contributions*, 1719, 1550
- . 2012b, *Icarus*, 221, 328

- Cloutis, E. A., Hudon, P., Romanek, C. S., et al. 2010, *Meteor. Planet. Sci.*, 45, 1668
- Cochran, A. L., & Barker, E. S. 1984, *Icarus*, 59, 296
- Delbo, M., Libourel, G., Wilkerson, J., et al. 2014, *Nature*, 508, 233
- de León, J., Campins, H., Tsiganis, K., Morbidelli, A., & Licandro, J. 2010, *A&A*, 513, A26
- Dermawan, B. 2004, PhD thesis, School of Science, University of Tokyo, pp. 118
- Dundon, L. 2005, Master’s thesis, University of Hawaii, pp. 66
- Fujiwara, A., & Tsukamoto, A. 1981, *Icarus*, 48, 329
- Gaftonyuk, N. M., Krugly, Yu. N., & Molotov, I. E. 2010, in *Protecting the Earth against Collisions with Asteroids and Comet Nuclei, Proceedings of the International Conference “Asteroid-Comet Hazard-2009”*, ed. A. M. Finkelstein, W. F. Huebner, & V. A. Shor (St. Petersburg: Nauka), 49–51, held in St. Petersburg, Russia, September 21–25, 2009
- Galushina, T. Yu., Ryabova, G. O., & Skripnichenko, P. V. 2015, *Planet. Space Sci.*, 118, 296
- Gladman, B., Migliorini, F., Morbidelli, A., et al. 1997, *Science*, 277, 197
- Granvik, M., Morbidelli, A., Jedicke, R., et al. 2016, *Nature*, 530, 303
- Green, S. F., & Kowal, C. 1983, *IAU Circ.*, 3878, #1
- Greenwood, R. C., Franchi, I. A., Kearsley, A. T., & Alard, O. 2010, *Geochim. Cosmochim. Acta*, 74, 1684
- Hamane, T., Kawakita, H., Kinugasa, K., Yamamuro, T., & Takeyama, N. 2002, *Publ. Astron. Soc. Japan*, 54, L35

- Hanuš, J., Delbo', M., Vokrouhlický, D., et al. 2016a, *A&A*, 592, A34
- . 2016b, DPS meeting, 48, 516.08
- Harris, A. W. 1998, *Icarus*, 131, 291
- Hicks, M. D., Fink, U., & Grundy, W. M. 1998, *Icarus*, 133, 69
- Hiroi, T., Pieters, C. M., Zolensky, M. E., & Lipschutz, M. E. 1993, *Science*, 261, 1016
- Hiroi, T., Zolensky, M. E., Pieters, C. M., & Lipschutz, M. E. 1996, *Meteor. Planet. Sci.*, 31, 321
- Hsieh, H., & Jewitt, D. 2005, *ApJ*, 624, 1093
- Hui, M.-T., & Li, J. 2017, *AJ*, 153, 23
- Ito, T., & Malhotra, R. 2010, *A&A*, 519, A63
- Jenniskens, P., Shaddad, M. H., Numan, D., et al. 2009, *Nature*, 485, 485
- Jewitt, D. 2013, *AJ*, 145, 133
- Jewitt, D., & Hsieh, H. 2006, *AJ*, 132, 1624
- Jewitt, D., Hsieh, H., & Agarwal, J. 2015, in *Asteroids IV*, ed. P. Michel, F. E. Demeo, & W. F. Bottke (Tucson, Arizona: The University of Arizona Press), 221–241
- Jewitt, D., & Li, J. 2010, *AJ*, 140, 1519
- Jewitt, D., Li, J., & Agarwal, J. 2013, *ApJ*, 771, L36
- Kaasalainen, S., Kaasalainen, M., & Piironen, J. 2005, *A&A*, 440, 1177
- Kadono, T., Arakawa, M., Ito, T., & Ohtsuki, K. 2009, *Icarus*, 200, 694

- Kasuga, T. 2009, *Earth, Moon, and Planets*, 105, 321
- Kasuga, T., & Jewitt, D. 2008, *AJ*, 136, 881
- Kasuga, T., Watanabe, J.-I., & Sato, M. 2006, *MNRAS*, 373, 1107
- Kinoshita, D., Ohtsuka, K., Sekiguchi, T., et al. 2007, *A&A*, 466, 1153
- Krugly, Yu. N., Belskaya, I. N., Shevchenko, V. G., et al. 2002, *Icarus*, 158, 294
- Krugly, Yu. N., Gaftonyuk, N. M., Belskaya, I. N., et al. 2007, in *Proceedings of the IAU Symposium No. 236*, Vol. 236, *Near Earth Objects, our Celestial Neighbors: Opportunity and Risk*, ed. A. Milani, G. B. Valsecchi, & D. Vokrouhlický (Cambridge: Cambridge University Press), 385–390, held in 14–18 August 2006, Praha, Czech Republic
- Lauretta, D. S., Bartels, A. E., Barucci, M. A., et al. 2015, *Meteor. Planet. Sci.*, 50, 834
- Lazzarin, M., Barucci, M. A., & Doressoundiram, A. 1996, *Icarus*, 122, 122
- Lebofsky, L. A., & Spencer, J. R. 1989, in *Asteroids II*, ed. R. P. Binzel, T. Gehrels, & M. S. Matthews (Tucson, Arizona: The University of Arizona Press), 128–147
- Li, J., & Jewitt, D. 2013, *AJ*, 145, 154
- Licandro, J., Campins, H., Mothé-Diniz, T., Pinilla-Alonso, N., & de León, J. 2007, *A&A*, 461, 751
- Luu, J. X., & Jewitt, D. C. 1990, *AJ*, 99, 1985
- Madiedo, J. M., Trigo-Rodríguez, J. M., Castro-Tirado, A. J., Ortiz, J. L., & Cabrera-Caño, J. 2013, *MNRAS*, 436, 2818
- Mann, I., Kimura, H., Biesecker, D. A., et al. 2004, *Space Sci. Rev.*, 110, 269

- Matsuoka, M., Nakamura, T., Kimura, Y., et al. 2015, *Icarus*, 254, 135
- Meech, K. J., Hainaut, O. R., Buie, M. W., A'Hearn, M., & Lisse, C. 1996, in *Abstracts of Asteroids, Comets, and Meteors 2016*, held in Versailles, France, 8–12 July, 1996
- Moroz, L., Baratta, G., Strazzulla, G., et al. 2004, *Icarus*, 170, 214
- Mothé-Diniz, T., Carvano, J. M., Bus, S. J., Duffard, R., & Burbine, T. H. 2008, *Icarus*, 195, 277
- Nakamura, T. 2005, *J. Miner. Petro. Sci.*, 100, 260
- . 2006, *Earth Planet. Sci. Lett.*, 242, 26
- Nakato, A., Nakamura, T., Kitajima, F., & Noguchi, T. 2008, *Earth, Planet, and Space*, 60, 855
- Nozaki, W., Nakamura, T., , & Noguchi, T. 2006, *Meteor. Planet. Sci.*, 41, 1095
- Ohtsuka, K., Arakida, H., Ito, T., Yoshikawa, M., & Asher, D. J. 2008, *Meteor. Planet. Sci. Supplement*, 43, 5055
- Ohtsuka, K., Nakato, A., Nakamura, T., et al. 2009, *Publ. Astron. Soc. Japan*, 61, 1375
- Ohtsuka, K., Sekiguchi, T., Kinoshita, D., et al. 2006, *A&A*, 450, L25
- Ohtsuka, K., Shimoda, C., Yoshikawa, M., & Watanabe, J.-I. 1997, *Earth, Moon, and Planets*, 77, 83
- Opeil, C. P., Consolmagno, G. J., & Britt, D. T. 2010, *Icarus*, 208, 449
- Pravec, P., Wolf, M., & Šarounová, L. 1998, *Icarus*, 136, 124
- Sarli, B. V., Kawakatsu, Y., & Arai, T. 2015, *J. Spacecraft and Rockets*, 52, 739

Tholen, D. J. 1985, IAU Circ., 4034, #2

Tomeoka, K., Kiriyama, K., Nakamura, K., Yamahana, Y., & Sekine, T. 2003, Nature, 423, 60

Urakawa, S., Ohtsuka, K., Abe, S., Ito, T., & Nakamura, T. 2014, AJ, 147, 121

Urakawa, S., Takahashi, S., Fujii, Y., et al. 2002, in *Dust in the Solar System and Other Planetary Systems*, ed. S. F. Green, I. Williams, T. McDonneli, & N. McBride (Oxford: Pergamon), 83–86, proceedings of the IAU Colloquium 181 held at the University of Kent, Canterbury, UK, 4–10 April 2000 (COSPAR)

Vilas, F., & Gaffey, M. J. 1989, Science, 246, 790

Warner, B. D. 2015, Minor Planet Bulletin, 42, 115

Whipple, F. L. 1983, IAU Circ., 3881, #1

Zappalà, V. 1980, The Moon and the Planets, 23, 345

Table 1: Specification of the spectrograph Hiyoyu

collimating lens	focal length = 240 mm
camera lens	focal length = 200 mm
dispersion element	reflective grating 300 gr mm ⁻¹ (or 1200 gr mm ⁻¹)
slit size	390 ^{''} × 1.5 ^{''} (projected on the sky)
detector	1K-CCD Apogee AP-8 (Kodak KAF-1001E)
spectral resolution $R(\lambda/\Delta\lambda)$	~ 333.133 at $\lambda = 5000$ Å
spectral wavelength range	3800–7600 Å (or 5000–9000 Å)
wavelength calibration lamp	Fe-Ne-Ar hollow cathode lamp
slit viewer	SBIG ST-8 (for target acquisition and autoguiding)

Table 2. Log of the spectroscopic observations of Phaethon

Sp ID	Date	Midtime		Frame ID	Exp.	AM
		UT 2007	UT			
1130–01	Nov 30	17:51:01	3200Phaethon-2091obj	300	1.36	
1130–02	Nov 30	17:58:12	3200Phaethon-2092obj	300	1.33	
1130–03	Nov 30	18:04:24	3200Phaethon-2093obj	300	1.30	
1130–04	Nov 30	18:10:27	3200Phaethon-2094obj	300	1.28	
1130–05	Nov 30	18:16:50	3200Phaethon-2095obj	300	1.25	
1130–06	Nov 30	18:22:58	3200Phaethon-2096obj	300	1.23	
1130–07	Nov 30	18:36:08	3200Phaethon-2099obj	300	1.19	
1130–08	Nov 30	18:42:44	3200Phaethon-2100obj	300	1.17	
1130–09	Nov 30	18:50:15	3200Phaethon-2101obj	300	1.15	
1130–10	Nov 30	18:56:45	3200Phaethon-2102obj	300	1.13	
1130–11	Nov 30	19:03:09	3200Phaethon-2103obj	300	1.12	
1130–12	Nov 30	19:10:02	3200Phaethon-2104obj	300	1.10	
1130–13	Nov 30	19:24:40	3200Phaethon-2107obj	300	1.08	
1130–14	Nov 30	19:30:51	3200Phaethon-2108obj	300	1.07	
1130–15	Nov 30	19:36:58	3200Phaethon-2109obj	300	1.06	
1130–16	Nov 30	19:43:14	3200Phaethon-2110obj	300	1.05	
1130–17	Nov 30	19:49:35	3200Phaethon-2111obj	300	1.04	
1130–18	Nov 30	19:55:43	3200Phaethon-2112obj	300	1.03	
1130–19	Nov 30	20:16:55	3200Phaethon-2115obj	300	1.02	
1130–20	Nov 30	20:23:08	3200Phaethon-2116obj	300	1.01	
1130–21	Nov 30	20:29:07	3200Phaethon-2117obj	300	1.01	
1130–22	Nov 30	20:35:07	3200Phaethon-2118obj	300	1.01	
1130–23	Nov 30	20:41:16	3200Phaethon-2119obj	300	1.00	
1130–24	Nov 30	20:47:28	3200Phaethon-2120obj	300	1.00	

Table 2—Continued

Sp ID	Date	Midtime		Frame ID	Exp.	AM
		UT 2007	UT			
1201-01	Dec 01	17:10:42	3200Phaethon-2067obj	300	1.68	
1201-02	Dec 01	17:17:24	3200Phaethon-2068obj	300	1.63	
1201-03	Dec 01	17:24:04	3200Phaethon-2069obj	300	1.57	
1201-04	Dec 01	17:30:55	3200Phaethon-2070obj	300	1.53	
1201-05	Dec 01	17:37:26	3200Phaethon-2071obj	300	1.49	
1201-06	Dec 01	17:43:48	3200Phaethon-2072obj	300	1.44	
1201-07	Dec 01	18:03:41	3200Phaethon-2076obj	300	1.34	
1201-08	Dec 01	18:09:59	3200Phaethon-2077obj	300	1.31	
1201-09	Dec 01	18:16:13	3200Phaethon-2078obj	300	1.29	
1201-10	Dec 01	18:22:53	3200Phaethon-2079obj	300	1.26	
1201-11	Dec 01	18:34:42	3200Phaethon-2082obj	300	1.22	
1201-12	Dec 01	18:41:25	3200Phaethon-2083obj	300	1.20	
1201-13	Dec 01	18:48:23	3200Phaethon-2084obj	300	1.18	
1201-14	Dec 01	18:54:46	3200Phaethon-2085obj	300	1.16	
1201-15	Dec 01	19:01:25	3200Phaethon-2086obj	300	1.14	
1201-16	Dec 01	19:07:50	3200Phaethon-2087obj	300	1.13	
1201-17	Dec 01	19:35:50	3200Phaethon-2096obj	300	1.07	
1201-18	Dec 01	19:42:22	3200Phaethon-2097obj	300	1.06	
1201-19	Dec 01	19:48:58	3200Phaethon-2098obj	300	1.05	
1201-20	Dec 01	19:55:35	3200Phaethon-2099obj	300	1.04	
1201-21	Dec 01	20:01:47	3200Phaethon-2100obj	300	1.04	
1201-22	Dec 01	20:08:03	3200Phaethon-2101obj	300	1.03	
1201-23	Dec 01	20:38:09	3200Phaethon-2110obj	300	1.01	
1201-24	Dec 01	20:44:19	3200Phaethon-2111obj	300	1.00	

Table 2—Continued

Sp ID	Date	Midtime	Frame ID	Exp.	AM
				UT 2007	UT
1201-25	Dec 01	20:51:15	3200Phaethon-2112obj	300	1.00
1201-26	Dec 01	20:58:41	3200Phaethon-2113obj	300	1.00
1201-27	Dec 01	21:04:41	3200Phaethon-2114obj	300	1.00
1202-01	Dec 02	18:11:07	3200Phaethon-2047obj	300	1.36
1202-02	Dec 02	18:23:17	3200Phaethon-2049obj	300	1.30
1202-03	Dec 02	18:29:21	3200Phaethon-2050obj	300	1.28
1202-04	Dec 02	18:35:28	3200Phaethon-2051obj	300	1.26
1202-05	Dec 02	18:41:53	3200Phaethon-2052obj	300	1.23
1202-06	Dec 02	19:13:40	3200Phaethon-2065obj	300	1.14
1202-07	Dec 02	19:19:29	3200Phaethon-2066obj	300	1.12
1202-08	Dec 02	19:25:38	3200Phaethon-2067obj	300	1.11
1202-09	Dec 02	19:32:25	3200Phaethon-2068obj	300	1.10
1202-10	Dec 02	19:38:54	3200Phaethon-2069obj	300	1.08
1202-11	Dec 02	19:45:04	3200Phaethon-2070obj	300	1.07
1202-12	Dec 02	20:13:00	3200Phaethon-2081obj	300	1.04
1202-13	Dec 02	20:18:58	3200Phaethon-2082obj	300	1.03
1202-14	Dec 02	20:25:17	3200Phaethon-2083obj	300	1.02
1202-15	Dec 02	20:31:46	3200Phaethon-2084obj	300	1.02
1202-16	Dec 02	20:37:53	3200Phaethon-2085obj	300	1.01
1202-17	Dec 02	20:43:43	3200Phaethon-2086obj	300	1.01

Note to the column heads.

Sp ID: spectrum ID,

Date and Midtime: observed date in 2007 and midtime of exposure (in UT),

Frame ID: Lulin spectral file ID in (hyyyymmdd_)OBJ-NO.fits,

Exp.: exposure (in second),

AM: airmass.

Table 3. Results of the VIS-spectrophotometries of Phaethon along with their geometries

Sp ID	JDT 2454430+	Δ AU	r AU	α deg	ϕ_K deg	ϕ_A deg	ϕ_H deg	S' %/0.1 μ m
1130-01	5.24452	0.2357	1.0862	59.11	-43.22	-28.88	-61.86	-6.70 ± 0.53
1130-02	5.24951	0.2356	1.0862	59.13	-43.21	-28.87	-61.86	-11.45 ± 1.25
1130-03	5.25381	0.2356	1.0861	59.14	-43.20	-28.86	-61.86	-7.86 ± 0.86
1130-04	5.25801	0.2355	1.0860	59.15	-43.19	-28.85	-61.86	-9.20 ± 0.50
1130-05	5.26245	0.2354	1.0860	59.16	-43.18	-28.84	-61.86	-7.49 ± 0.70
1130-06	5.26671	0.2353	1.0859	59.17	-43.17	-28.83	-61.86	-8.31 ± 0.42
1130-07	5.27585	0.2352	1.0857	59.19	-43.14	-28.81	-61.86	-6.82 ± 1.56
1130-08	5.28043	0.2351	1.0857	59.20	-43.13	-28.80	-61.86	-6.90 ± 0.40
1130-09	5.28565	0.2350	1.0856	59.21	-43.12	-28.79	-61.86	-7.91 ± 0.57
1130-10	5.29017	0.2349	1.0855	59.22	-43.11	-28.78	-61.86	-6.24 ± 0.83
1130-11	5.29461	0.2348	1.0855	59.23	-43.10	-28.77	-61.86	0.30 ± 1.53
1130-12	5.29939	0.2347	1.0854	59.24	-43.09	-28.75	-61.86	-3.23 ± 0.91
1130-13	5.30955	0.2345	1.0852	59.27	-43.06	-28.73	-61.86	-3.53 ± 0.34
1130-14	5.31385	0.2345	1.0851	59.28	-43.05	-28.72	-61.86	-7.17 ± 0.66
1130-15	5.31810	0.2344	1.0851	59.29	-43.04	-28.71	-61.86	-3.07 ± 0.35
1130-16	5.32245	0.2343	1.0850	59.30	-43.03	-28.70	-61.86	-2.31 ± 0.73
1130-17	5.32686	0.2342	1.0849	59.31	-43.02	-28.69	-61.86	-2.57 ± 0.60
1130-18	5.33112	0.2341	1.0849	59.32	-43.01	-28.68	-61.86	-4.24 ± 0.62
1130-19	5.34584	0.2339	1.0846	59.35	-42.97	-28.64	-61.86	-4.36 ± 0.32
1130-20	5.35016	0.2338	1.0846	59.36	-42.96	-28.63	-61.86	-0.00 ± 0.30
1130-21	5.35431	0.2337	1.0845	59.37	-42.95	-28.62	-61.86	-1.08 ± 0.26
1130-22	5.35848	0.2336	1.0844	59.38	-42.94	-28.61	-61.86	-2.64 ± 0.48
1130-23	5.36275	0.2336	1.0844	59.39	-42.93	-28.60	-61.86	-3.83 ± 0.23
1130-24	5.36705	0.2335	1.0843	59.40	-42.92	-28.59	-61.86	-2.99 ± 0.22

Table 3—Continued

Sp ID	JDT 2454430+	Δ AU	r AU	α deg	ϕ_K deg	ϕ_A deg	ϕ_H deg	S' %/0.1 μ m
1201-01	6.21652	0.2182	1.0709	61.62	-40.67	-26.43	-61.69	-6.38 \pm 0.45
1201-02	6.22117	0.2181	1.0708	61.63	-40.66	-26.42	-61.69	-10.26 \pm 0.45
1201-03	6.22580	0.2180	1.0708	61.64	-40.64	-26.40	-61.69	-4.11 \pm 0.37
1201-04	6.23056	0.2179	1.0707	61.66	-40.63	-26.39	-61.69	-3.90 \pm 0.34
1201-05	6.23509	0.2179	1.0706	61.67	-40.62	-26.38	-61.69	-4.45 \pm 0.48
1201-06	6.23951	0.2178	1.0705	61.68	-40.61	-26.37	-61.69	-5.25 \pm 0.34
1201-07	6.25332	0.2175	1.0703	61.72	-40.57	-26.33	-61.68	-2.96 \pm 0.34
1201-08	6.25769	0.2175	1.0703	61.73	-40.55	-26.32	-61.68	-1.33 \pm 0.41
1201-09	6.26202	0.2174	1.0702	61.74	-40.54	-26.30	-61.68	0.63 \pm 0.43
1201-10	6.26665	0.2173	1.0701	61.76	-40.53	-26.29	-61.68	-1.10 \pm 0.28
1201-11	6.27485	0.2172	1.0700	61.78	-40.50	-26.27	-61.67	-0.26 \pm 0.32
1201-12	6.27952	0.2171	1.0699	61.79	-40.49	-26.26	-61.67	-3.05 \pm 0.28
1201-13	6.28436	0.2170	1.0698	61.80	-40.48	-26.24	-61.67	-2.40 \pm 0.33
1201-14	6.28879	0.2169	1.0698	61.82	-40.46	-26.23	-61.67	-4.28 \pm 0.33
1201-15	6.29341	0.2168	1.0697	61.83	-40.45	-26.22	-61.67	-3.69 \pm 0.31
1201-16	6.29786	0.2167	1.0696	61.84	-40.44	-26.21	-61.67	-1.91 \pm 0.28
1201-17	6.31731	0.2164	1.0693	61.90	-40.38	-26.15	-61.66	1.22 \pm 0.40
1201-18	6.32185	0.2163	1.0692	61.91	-40.37	-26.14	-61.66	1.59 \pm 0.40
1201-19	6.32643	0.2162	1.0692	61.92	-40.36	-26.13	-61.66	-0.02 \pm 1.96
1201-20	6.33102	0.2162	1.0691	61.94	-40.34	-26.11	-61.65	2.67 \pm 0.35
1201-21	6.33533	0.2161	1.0690	61.95	-40.33	-26.10	-61.65	1.58 \pm 0.39
1201-22	6.33968	0.2160	1.0690	61.96	-40.32	-26.09	-61.65	1.82 \pm 0.36
1201-23	6.36058	0.2156	1.0686	62.02	-40.26	-26.03	-61.64	-1.40 \pm 0.31
1201-24	6.36487	0.2156	1.0686	62.03	-40.24	-26.02	-61.64	-1.60 \pm 1.01

Table 3—Continued

Sp ID	JDT 2454430+	Δ AU	r AU	α deg	ϕ_K deg	ϕ_A deg	ϕ_H deg	S' %/0.1 μm
1201–25	6.36968	0.2155	1.0685	62.04	−40.23	−26.01	−61.64	0.36 ± 0.32
1201–26	6.37484	0.2154	1.0684	62.06	−40.22	−25.99	−61.64	0.44 ± 0.25
1201–27	6.37901	0.2153	1.0683	62.07	−40.20	−25.98	−61.64	0.62 ± 0.32
1202–01	7.25848	0.2001	1.0543	64.81	−37.43	−23.32	−61.11	5.23 ± 0.54
1202–02	7.26693	0.1999	1.0541	64.84	−37.40	−23.29	−61.11	4.37 ± 1.45
1202–03	7.27114	0.1998	1.0541	64.85	−37.39	−23.28	−61.10	3.95 ± 0.43
1202–04	7.27539	0.1998	1.0540	64.87	−37.38	−23.26	−61.10	5.86 ± 0.29
1202–05	7.27984	0.1997	1.0539	64.88	−37.36	−23.25	−61.09	6.63 ± 0.26
1202–06	7.30191	0.1993	1.0536	64.96	−37.29	−23.18	−61.08	−7.23 ± 0.44
1202–07	7.30595	0.1993	1.0535	64.97	−37.27	−23.16	−61.07	−6.44 ± 0.41
1202–08	7.31023	0.1992	1.0534	64.98	−37.26	−23.15	−61.07	−8.05 ± 0.34
1202–09	7.31494	0.1991	1.0534	65.00	−37.24	−23.13	−61.07	−8.35 ± 0.43
1202–10	7.31944	0.1990	1.0533	65.01	−37.23	−23.12	−61.06	−6.28 ± 0.51
1202–11	7.32372	0.1990	1.0532	65.03	−37.21	−23.11	−61.06	−6.22 ± 0.27
1202–12	7.34312	0.1986	1.0529	65.09	−37.14	−23.04	−61.04	−5.67 ± 0.26
1202–13	7.34726	0.1986	1.0528	65.11	−37.13	−23.03	−61.04	−7.35 ± 0.22
1202–14	7.35165	0.1985	1.0528	65.12	−37.11	−23.01	−61.03	−6.40 ± 0.27
1202–15	7.35615	0.1984	1.0527	65.14	−37.10	−23.00	−61.03	−6.89 ± 0.26
1202–16	7.36040	0.1983	1.0526	65.15	−37.08	−22.98	−61.03	−4.23 ± 1.83
1202–17	7.36445	0.1983	1.0526	65.17	−37.07	−22.97	−61.02	−5.78 ± 0.39

Note to the column heads.

Sp ID: spectrum ID,

JDT: Julian Terrestrial Date,

Δ and r : geocentric and heliocentric distances (in AU),

α : phase angle (in degree),

ϕ_K , ϕ_A , and ϕ_H : sub-Earth latitudes (in degree), based on the pole solutions, SOL K by Krugly et al. (2002), SOL A by Ansdell et al. (2014), and SOL H by Hanuš et al. (2016a), respectively,

S' : spectral gradient (in %/0.1 μm).

Table 4. Pole axis parameters of Phaethon’s rotation for the geometric analyses

Solution	λ_P	β_P	P	# Nights	Arc
ID	deg	deg	hr		
SOL K	97 ± 15	-11 ± 15	3.5904399 ± 0.000002	6	1996 Sep–1997 Nov
SOL A	85 ± 13	-20 ± 10	3.6032 ± 0.0008	15	1994 Dec 27–2013 Dec 11
SOL H	319 ± 5	-39 ± 5	3.603958 ± 0.000002	49	1994 Nov 02–2015 Oct 08

References to solution ID.

SOL K (Krugly et al. 2002), SOL A (Ansdell et al. 2014), and SOL H (Hanuš et al. 2016a).

Note to the column heads.

λ_P and β_P : ecliptic longitude and latitude (in degree, equinox J2000) of pole axis orientation,

P : sidereal rotation period (in hour),

Nights and Arc: number of observed night and its photometric arc, taken in the pole axis determination.

Table 5. Other VIS-spectroscopic data of Phaethon

Sp ID	Date	Δ	r	α	ϕ_K	ϕ_A	ϕ_H	S'	EWR	Tel.
		UT	AU	AU	deg	deg	deg	deg	μm	
CB1983	1983 Dec 02	1.16	1.67	35.0	16.6	10.0	16.3	23.0	0.36–0.64	HJS 2.7m
LJ1988	1988 Oct 06	1.75	2.38	21.8	−53.8	−51.2	−30.2	−11.0	0.36–0.72	KPNO 2.1m
Ch1993	1993 Oct 21	0.43	0.99	78.0	44.4	52.8	−12.8	−4.0	0.36–0.62	Perkins 1.8m
La1994	1994 Oct 10	1.49	1.99	29.0	−65.9	−57.0	−40.3	−3.9	0.38–1.00	CFHT 3.6m
8	1994 Nov 15	0.81	1.71	20.0	−61.0	−54.3	−38.2	−1.7	0.44–0.93	MDM 2.4m
Hi1995	1995 Nov 26	1.49	2.40	12.0	−27.6	−31.5	−8.3	−1.8	0.55–0.95	Kuiper 1.54m
sp19	2002 Oct 27	1.37	2.28	13.0	−31.8	−33.2	−17.4	−2.1	0.44–0.93	MIT-SMASS
Li2003	2003 Nov 14.8	0.72	1.18	56.9	47.3	42.8	16.4	−4.0	0.52–0.95	WHT 4.2m
sp34	2004 Dec 10	0.64	1.58	17.0	−40.3	−43.4	−14.6	−2.2	0.44–0.93	MIT-SMASS
Li2004a	2004 Dec 21.0	0.61	1.46	30.9	−29.5	−35.5	−2.5	−4.0	0.35–0.60	NOT 2.5m
Li2004b	2004 Dec 21.0	0.61	1.46	30.9	−29.5	−35.5	−2.5	−4.0	0.60–0.90	NOT 2.5m
sp204n1	2014 Nov 28	0.85	1.81	9.3	−47.5	−47.8	−23.0	−2.1	0.44–0.93	MIT-SMASS
sp204n2	2014 Nov 29	0.84	1.80	9.4	−46.8	−47.4	−22.2	−2.1	0.44–0.93	MIT-SMASS
dm19n2	2014 Dec 02	0.82	1.78	10.4	−44.7	−46.1	−19.9	−2.1	0.44–0.93	MIT-SMASS
4								−6.8	0.36–0.93	Palomar 5m

References to Sp ID (spectrum ID).

CB1983 (Cochran & Barker 1984), LJ1988 (Luu & Jewitt 1990), Ch1996 (Chamberlin et al. 1996), La1994 (Lazzarin et al. 1996), 8 (Binzel et al. 2004), Hi1995 (Hicks et al. 1998), sp19, 34, 204n1, 204n2, and dm19n2 (MIT–UH–IRTF Joint Campaign for NEO Reconnaissance, see <http://smass.mit.edu/smash.html>), Li2003, 2004a, and 2004b (Licandro et al. 2007), and 4 (Binzel et al. 2001, whose time data were not given in).

Note to the column heads.

Date: date and time of the observation (in UT),

Δ and r : geocentric and heliocentric distances (in AU),

α : phase angle (in degree),

ϕ_K , ϕ_A , and ϕ_H : sub-Earth latitudes (in degree), based on SOLs K, A, and H, respectively,

S' : spectral gradient (in %/0.1 μm),

EWR: effective wavelength range of the spectrum (in μm),

Tel.: telescope used in the observation.

Table 6. VIS-spectroscopic data of metamorphosed carbonaceous chondrites from the RELAB database

Name	Type	Sample ID	Heated at	Gr. size	S'	Remark
				°C	μm	
Y-82162	CI-an	MB-CMP-019-1		< 125	1.67 ± 0.01	
		MB-CMP-019-C		chip	-0.32 ± 0.03	interior chip
Ivuna	CI1	MP-TXH-018-F	100	< 125	9.74 ± 0.05	heated for 1 week
		MP-TXH-018-G	200	< 125	5.18 ± 0.02	heated for 1 week
		MP-TXH-018-A	300	< 125	4.08 ± 0.01	heated for 1 week
		MP-TXH-018-B	400	< 125	6.41 ± 0.02	heated for 1 week
		MP-TXH-018-C	500	< 125	5.58 ± 0.01	heated for 1 week
		MP-TXH-018-D	600	< 125	4.05 ± 0.01	heated for 1 week
		MP-TXH-018-E	700	< 125	-4.24 ± 0.02	heated for 1 week
		MB-TXH-064-2		< 125	8.50 ± 0.18	
Murchison	CM2	MB-TXH-064-3		< 63	9.33 ± 0.18	
		MB-TXH-064-4		63–125	6.21 ± 0.14	
		MB-TXH-064-A	400	< 63	13.44 ± 0.03	heated for 1 week
		MB-TXH-064-B	500	< 63	11.42 ± 0.02	heated for 1 week
		MB-TXH-064-C	600	< 63	5.76 ± 0.01	heated for 1 week
		MB-TXH-064-D	700	< 63	3.24 ± 0.02	heated for 1 week
		MB-TXH-064-E	800	< 63	3.29 ± 0.02	heated for 1 week
		MB-TXH-064-F	900	< 63	0.26 ± 0.01	heated for 1 week
		MB-TXH-064-G	1000	< 63	1.44 ± 0.02	heated for 1 week
		MB-TXH-064-H	400	63–125	12.97 ± 0.03	heated for 1 week
		MB-TXH-064-I	500	63–125	9.81 ± 0.03	heated for 1 week
		MB-TXH-064-J	600	63–125	5.19 ± 0.01	heated for 1 week
		MB-TXH-064-K	700	63–125	1.84 ± 0.01	heated for 1 week
		MB-TXH-064-L	800	63–125	3.41 ± 0.02	heated for 1 week

Table 6—Continued

Name	Type	Sample ID	Heated at	Gr. size	S'	Remark
				°C	μm	
Murchison	CM2	MB-TXH-064-M	900	63–125	-0.98 ± 0.01	heated for 1 week
		MB-TXH-064-N		63–125	1.45 ± 0.02	heated for 1 week
B-7904	CM-an	MB-CMP-018-1		chip	6.82 ± 0.04	
Y-86720	CM-an	MB-CMP-020-1		< 125	2.49 ± 0.06	
		MB-CMP-020-A		chip	3.21 ± 0.09	smaller chip
		MB-CMP-020-B		chip	2.27 ± 0.07	larger chip
MET01070	CM1	PH-D2M-043		< 75	0.43 ± 0.08	
PCA02012	CM2	PH-D2M-044		< 75	28.85 ± 0.59	
Y-693	CK4	MB-TXH-077		< 125	6.73 ± 0.14	
ALH85002	CK4	MB-TXH-081-1		chip	3.52 ± 0.11	
		MB-TXH-081-2		< 125	2.88 ± 0.12	
		MB-TXH-081-A		< 25	5.18 ± 0.08	
		MB-TXH-081-B		25–45	2.66 ± 0.06	
		MB-TXH-081-C		45–75	0.34 ± 0.08	
		MB-TXH-081-D		75–125	1.31 ± 0.06	
		MH-FPF-058-A		< 180	4.72 ± 0.14	
EET92002	CK4	MH-FPF-058-B		< 180	7.29 ± 0.19	fusion-crusted
		MC-RPB-003		< 500	0.76 ± 0.11	
MET01149	CK3	PH-D2M-045		< 75	7.46 ± 0.26	
PCA91470	CK4	PH-D2M-046		< 75	3.94 ± 0.22	
EET83311	CK5	PH-D2M-047		< 75	5.83 ± 0.33	
DAV92300	CK4	PH-D2M-053		< 75	2.86 ± 0.08	

Note to the column heads.

Name: official meteorite name,

Type: classified meteorite type, in which XX-an means anomalous, and metamorphic,

Sample ID: from the RELAB database,

Heated at: experimentally heated temperature (in °C), in which the blank indicates unheated,

Gr. size: grain size (in μm),

S' : spectral gradient (in %/0.1 μm).

Table 7. VIS-NIR spectral features on Phaethon and its meteoritic analog candidates

Sample Name	Heated at	Gr. size	S'	UV/ B feature	0.7- μ m feature	1.05- μ m feature
	°C	μ m	%/0.1 μ m			
Phaethon	(< 800?)		> -11	very weak	no	no
Y-82162 (CI-an)	(< 750)	chip	-0.32	weak	no	no
Ivuna (CI1)	700	< 125	-4.24	very weak	no	no
Murchison (CM2)	900	63–125	-0.98	weak	no	no
CK chondrites	(300–1000)	various	positive	yes	no	yes

Note.

Heated temperature put in parenthesis means estimated temperature.

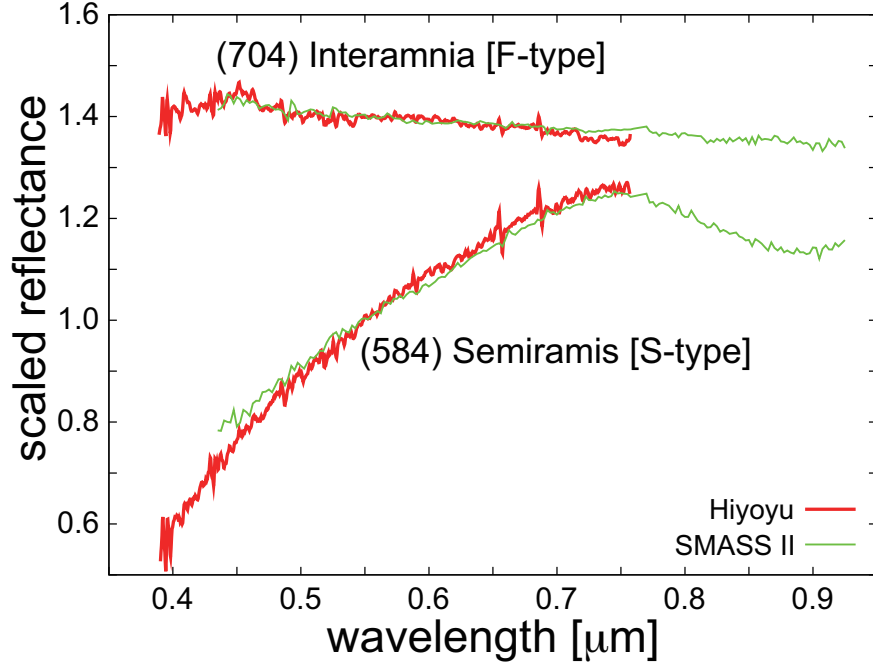


Fig. 1.— The VIS-spectra of (548) Semiramis and (704) Interamnia obtained by Hiyoyu, together with those from the SMASS II database for comparison. They are normalized at $0.55 \mu\text{m}$. The spectra of Interamnia are shifted by +0.4 in vertical direction. See Section 2.1 for more detail.

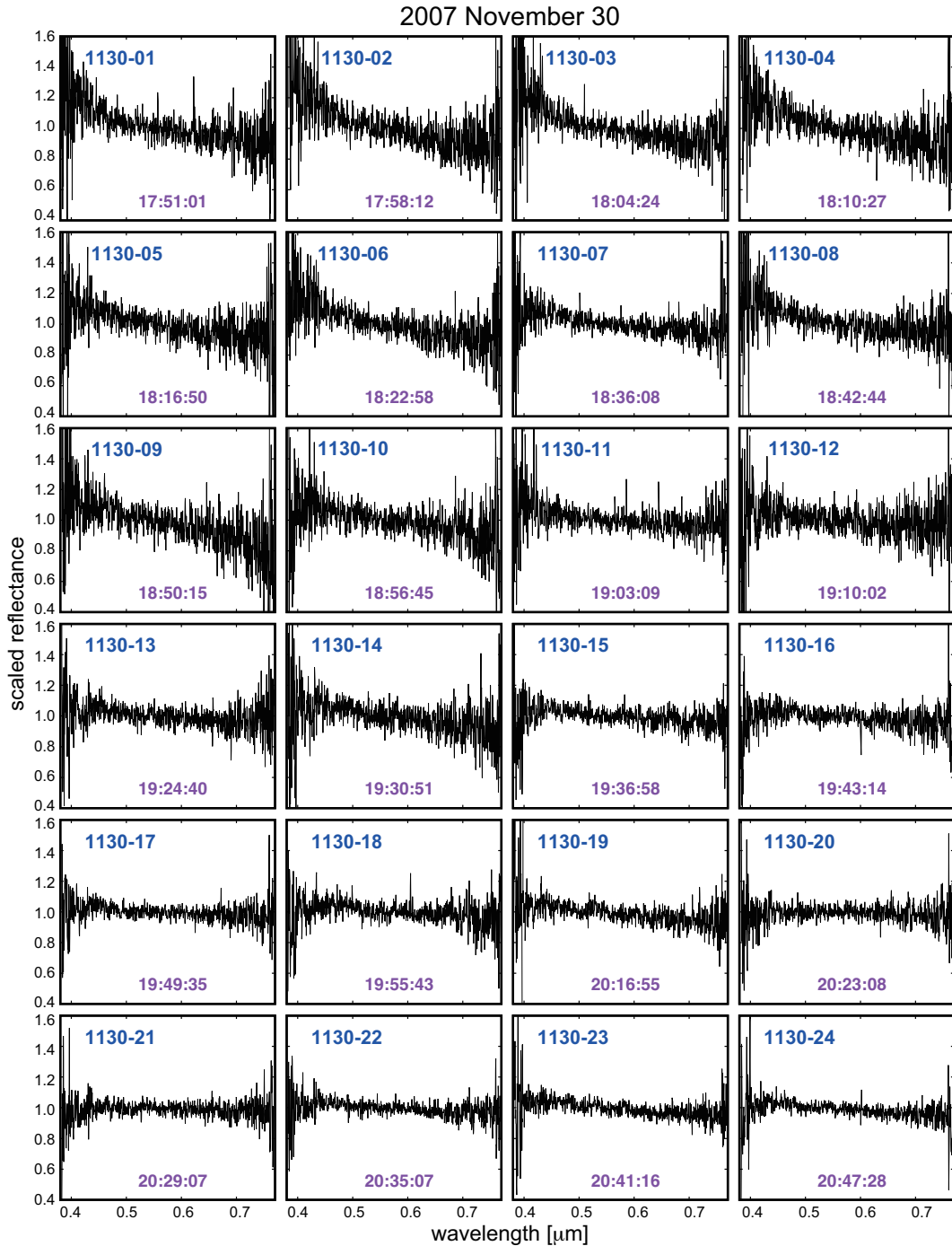


Fig. 2.— Time-series VIS-spectra of Phaethon recorded on 30 November, 2007.

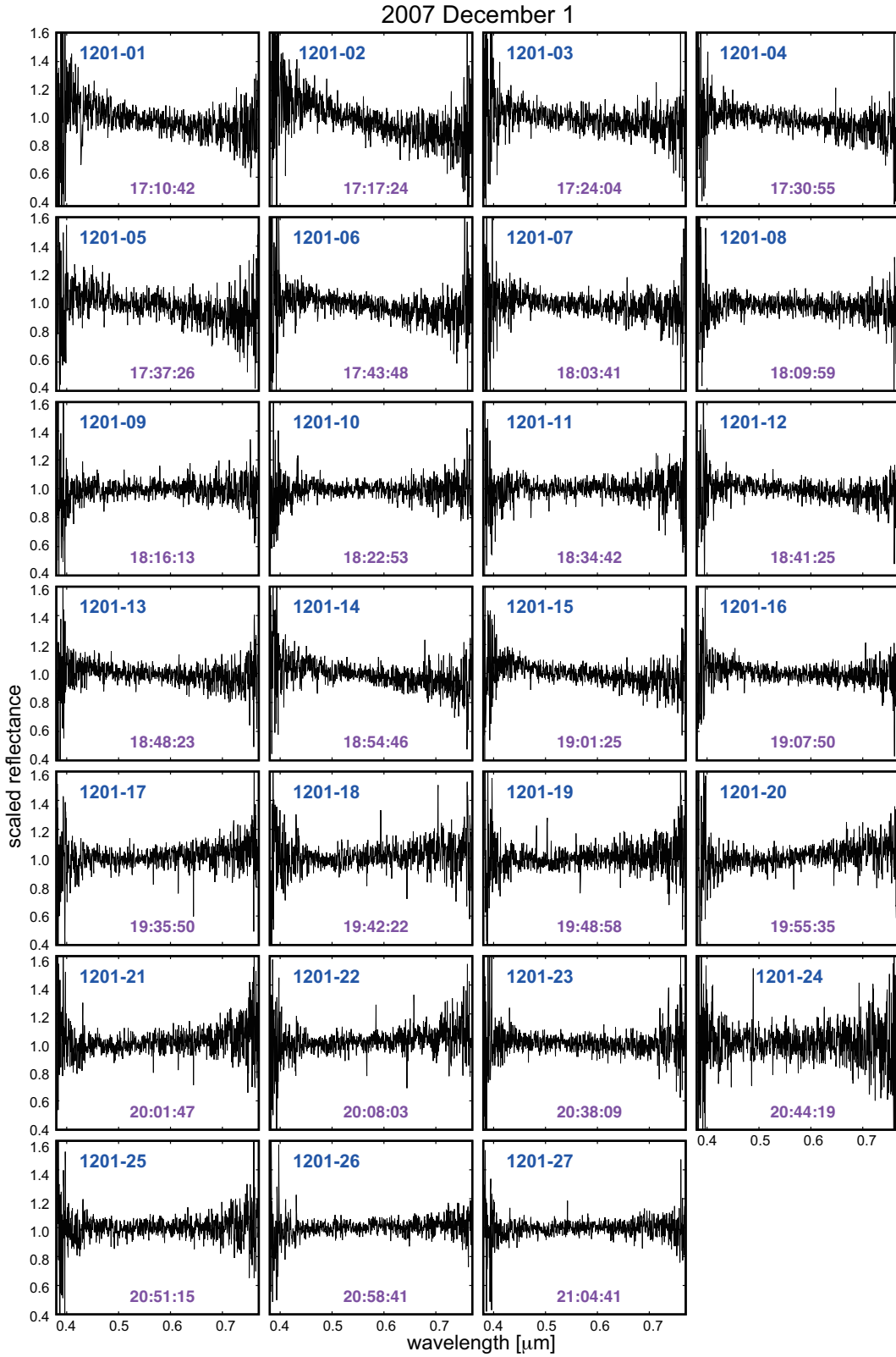


Fig. 3.— recorded on 1 December, 2007.

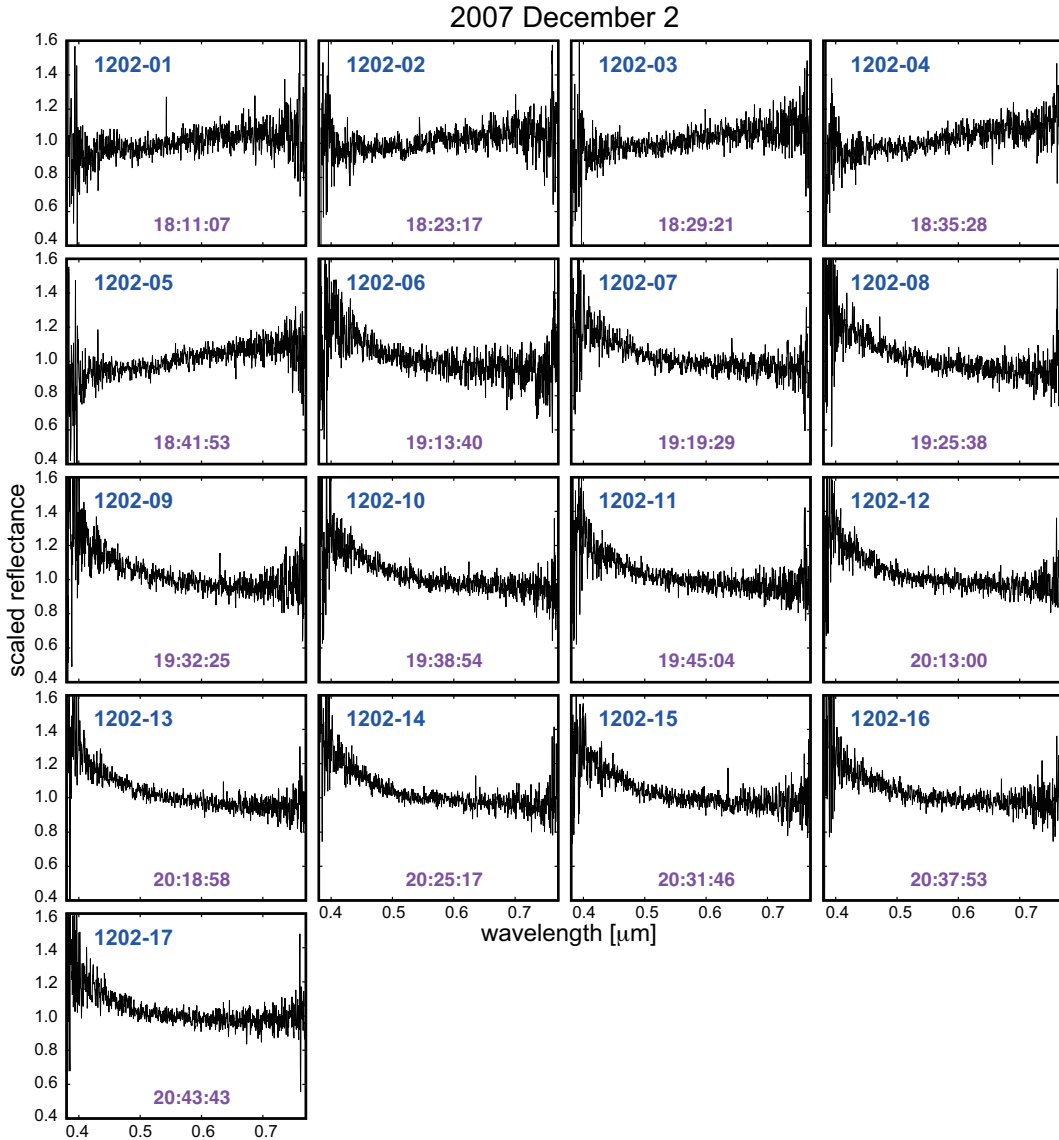


Fig. 4.— recorded on 2 December, 2007.

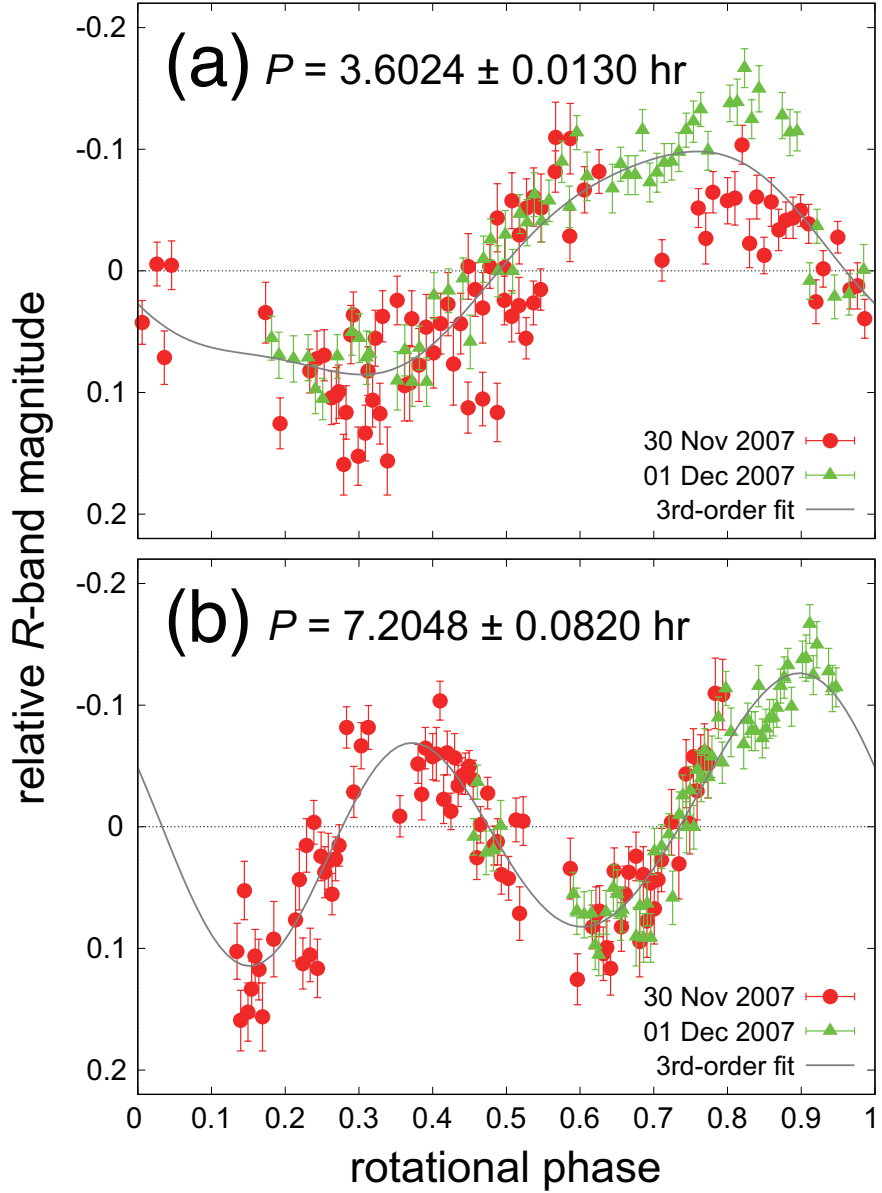


Fig. 5.— *R*-band photometries and rotational phase-curve fittings of Phaethon. Panel (a) shows the best fitted single-peaked lightcurve by phase-folding with $P = 3.6024 \pm 0.0130 \text{ hr}$; (b) the double-peaked lightcurve by phase-folding with $2P, 7.2048 \pm 0.0820 \text{ hr}$. The gray solid curves are results of the least-square fit by applying the 3rd-order Fourier harmonics. See Section 3.2 for more detail.

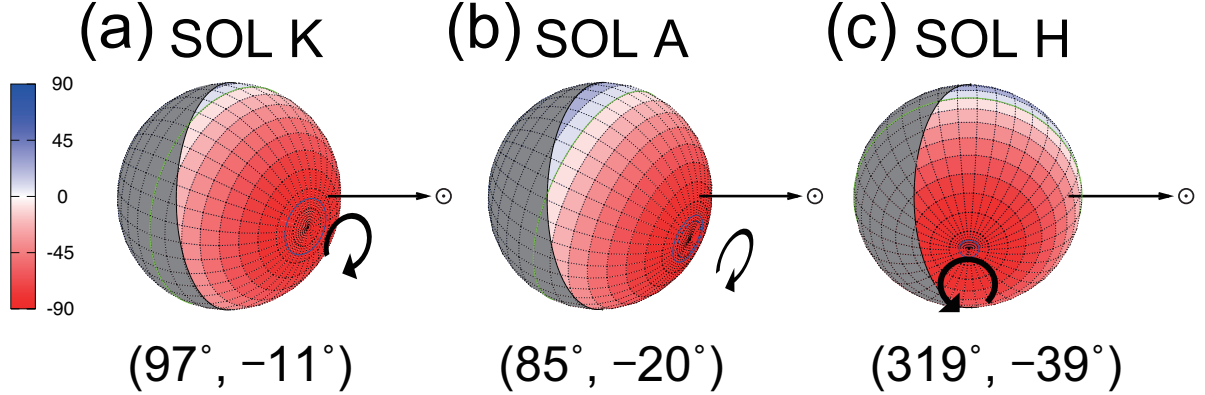


Fig. 6.— Schematic reconstructions of three geometric models of Phaethon as viewed from the Earth at the time of 19:35:50 UT, 1 December, 2007, at which the spectrum 1201-17 was recorded, i.e., near median time of our spectroscopic observations. Panel (a) is reconstructed from SOL K by Krugly et al. (2002) with description of pole coordinate (λ_P, β_P) , similarly (b) from SOL A of by Ansdell et al. (2014), and (c) from SOL H by Hanuš et al. (2016a). Then their aspect angles are $40^\circ.6S$, $26^\circ.3S$, and $61^\circ.7S$, respectively. The phase angle, α , was $61^\circ.90$, thus the ratio of the luminous area to the total area of disk, $k = 0.74$, where the gray area indicates the sun-shadow. The southern hemisphere faces to the Earth at the time of observation in every models. The arrow directs from the subsolar point to the Sun (symbolized by \odot), whose length is equal to Phaethon’s radius. The blue line means an error circle for every models.

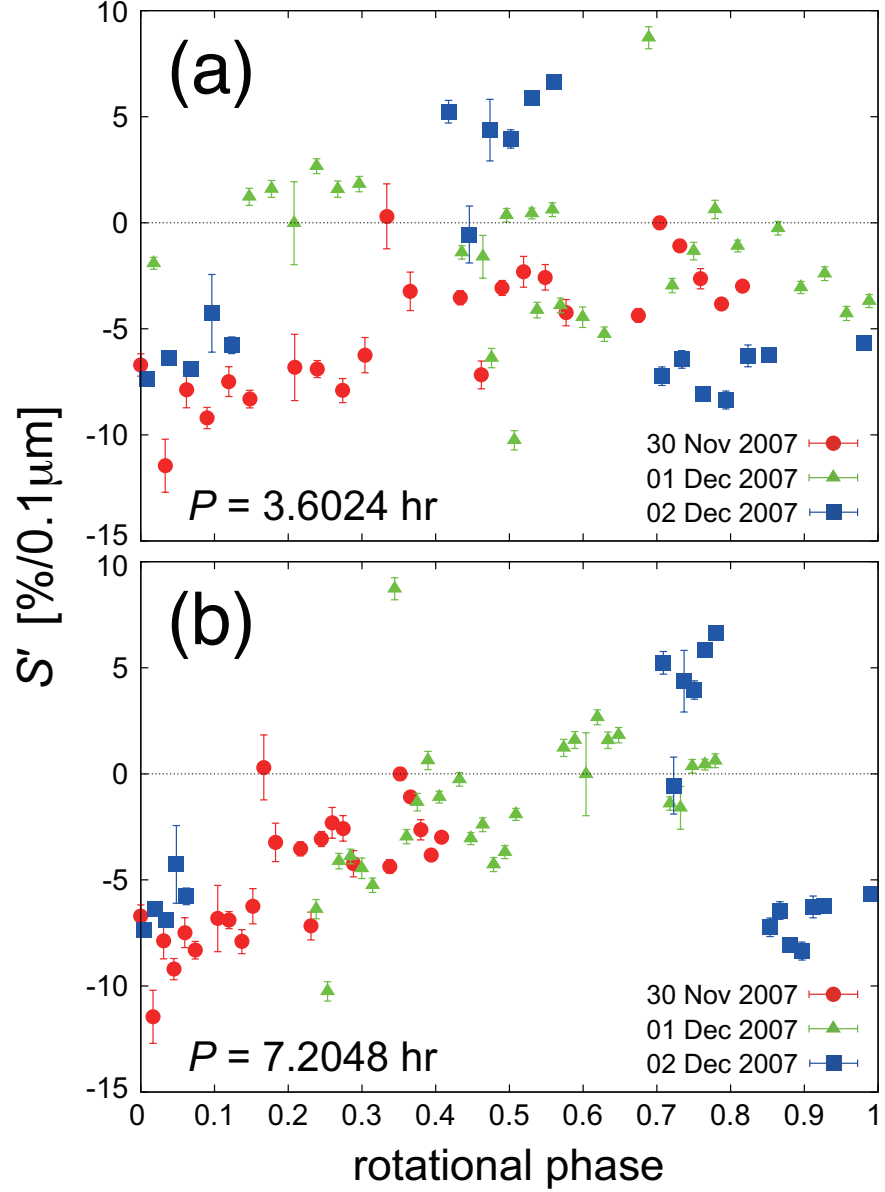


Fig. 7.— Potential correlation between spectral gradients, S' , of Phaethon and its rotational phase by phase-folding with $P = 3.6024$ hr for panel (a) and 7.2048 hr for (b). See Section 3.3 for more detail.

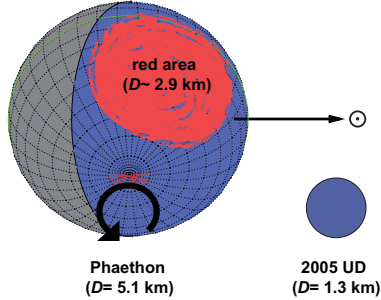


Fig. 8.— Conceptual scheme of the C-type red-colored area on Phaethon as viewed from the Earth at the time of which the spectrum 1202-01 ($S' = 5.23 \pm 0.54$) was recorded. The pole orientation is based on SOL H (Hanuš et al. 2016a). See Section 3.4 for more detail.

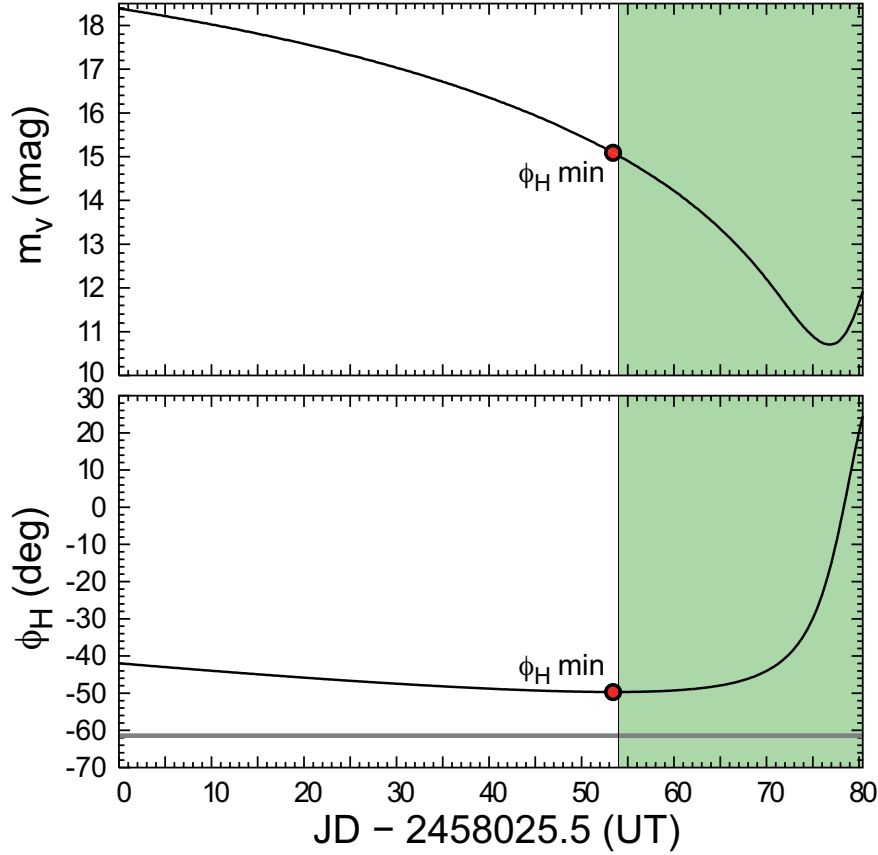


Fig. 9.— The time-variation of ϕ_H (lower panel) along with m_v (upper panel) in 2017. The abscissa is time in Julian Date (JD) since 29 September, 2017 (JD 2458025.5) up to 18 December, 2017 (JD 2458105.5), in which the observing conditions at a solar elongation of over 90° turn up. The horizontal gray lines between $61^\circ.02S$ to $61^\circ.86S$ indicate the geometric conditions of our spectrophotometries in 2007. The light-green zone in UT indicates the brightness of Phaethon to be $m_v < 15.0$ mag in 22 November–18 December, thus providing good observing conditions for spectrophotometry using the 2-m class telescopes. The aspect ϕ_H will reach down to minimum (=highest) at $49^\circ.7S$ on 21 November (marked by the red circle), in which the difference of ϕ_H with our VIS-spectroscopic observations in 2007 is only $\sim 12^\circ$. So, Phaethon will be observable in several days around 21 November, 2017 under similar geometric condition with the 2007 observations for testing our hypothesis.